Inorganic Chemistry

Article

pubs.acs.org/IC

Zwitterionic Cobalt Complexes with Bis(diphenylphosphino)(*N*-thioether)amine Assembling Ligands: Structural, EPR, Magnetic, and Computational Studies

Christophe Fliedel,[†] Vitor Rosa,[†] Bertrand Vileno,[‡,§] Nathalie Parizel,[‡] Sylvie Choua,[‡] Christophe Gourlaouen,[‖] Patrick Rosa,[⊥] Philippe Turek,[‡] and Pierre Braunstein*[,†]

[†]Laboratoire de Chimie de Coordination, [‡]Laboratoire POMAM, and [‖]Laboratoire de Chimie Quantique, Institut de Chimie (UMR 7177 CNRS), Université de Strasbourg, 4 rue Blaise Pascal, CS 90032, 67081 Strasbourg, France

[§]French EPR Federation of Research (REseau NAtional de Rpe interDisciplinaire, RENARD), Fédération IR-RPE CNRS 3443, 67081 Strasbourg, France

[⊥]CNRS, Université de Bordeaux, ICMCB, UPR9048, F-33600 Pessac, France

Ⓢ *Supporting Information*

ABSTRACT: The coordination of two heterofunctional *P,P,S* ligands of the *N*-functionalized DPPA-type bearing an alkylthioether or arylthioether *N*-substituent, (Ph$_2$P)$_2$N(CH$_2$)$_3$SMe (**1**) and (Ph$_2$P)$_2$N(*p*-C$_6$H$_4$)SMe (**2**), respectively, toward cobalt dichloride was investigated to examine the influence of the linker between the P*N*P nitrogen and the *S* atoms. The complexes [CoCl$_2$(**1**)]$_2$ (**3**) and [CoCl$_2$(**2**)]$_2$ (**4**) have been isolated, and **3** was shown by X-ray diffraction to be a unique dinuclear, zwitterion containing one CoCl moiety bis-chelated by two ligands **1** and one CoCl$_3$ fragment coordinated by the S atom of a thioether function. The FT-IR, UV−vis, and EPR spectroscopic features of **3** were analyzed as the superposition of those of constitutive fragments identified by a retrosynthetic-type analysis. A similar approach provided insight into the nature of **4** for which no X-ray diffraction data could be obtained. A comparison between the spectroscopic features of **4** and of its constitutive fragments, [CoCl(**2**)$_2$]PF$_6$ (**7**) and [H**2′**]$_2$[CoCl$_4$] (**8**) (**2′** = NH$_2$(*p*-C$_6$H$_4$)SMe), and between those of **4** and **3** suggested that **4** could either have a zwitterionic structure, similar to that of **3**, or contain a tetrahedral dicationic bis-chelated Co center associated with a CoCl$_4$ dianion. Magnetic and EPR studies and theoretical calculations were performed. Doublet spin states were found for the pentacoordinated complexes [CoCl(**1**)$_2$]PF$_6$ (**5**) and **7** and anisotropic quadruplet spin states for the tetrahedral complexes [CoCl$_3$(H**1′**)] (**6**) (**1′** = NH$_2$(CH$_2$)$_3$SMe) and **8**. A very similar behavior was observed for **3** and **4**, consisting in the juxtaposition of noninteracting doublet and quadruplet spin states. Antiferromagnetic interactions explain the formation of dimers for **6** and of layers for **8**. The EPR signatures of **3** and **4** correspond to the superposition of low-spin nuclei in **5** and **7** and high-spin nuclei in **6** and **8**, respectively. From DFT calculations, the solid-state structure of **4** appears best described as zwitterionic, with a low-spin state for the Co1 atom.

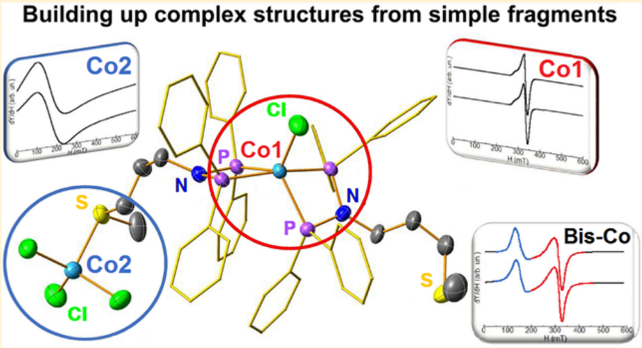

INTRODUCTION

The profuse chemistry of short-bite ligands, particularly the diphosphines bis(diphenylphosphino)methane (DPPM) and bis(diphenylphosphino)amine (DPPA) and their derivatives, magnified by the diversity of their coordination modes (monodentate, bridging, chelating), instigated a longstanding interest across the scientific community.[1] The versatility of DPPA-type ligands can be amplified by the introduction of various *N*-substituents and empowers an extensive number of applications, such as the formation of mono- or polynuclear complexes[2] or the anchoring of coordination compounds into mesoporous materials[3] or on metallic surfaces.[4] Metal complexes with such short-bite ligands are involved in various catalytic reactions,[5] and their Ni and Cr derivatives have been successfully applied to the catalytic oligo- or polymerization of ethylene.[6,7]

The study of the electronic structure of first-row transition metal ions in relation with their stereochemistry is a very relevant field in coordination and biological chemistry, and it is essential to analyze how stereochemistry, electronic structure, and magnetic properties correlate.[8,9] We became interested in the coordination chemistry of *N*-thioether-functionalized DPPA-type ligands, such as (Ph$_2$P)$_2$N(CH$_2$)$_3$SMe (**1**) and (Ph$_2$P)$_2$N(*p*-C$_6$H$_4$)SMe (**2**), with an alkyl or an aryl spacer, respectively (Chart 1, top) because of (i) the versatility of the

Received: December 14, 2015

DOI: 10.1021/acs.inorgchem.5b02889

Chart 1

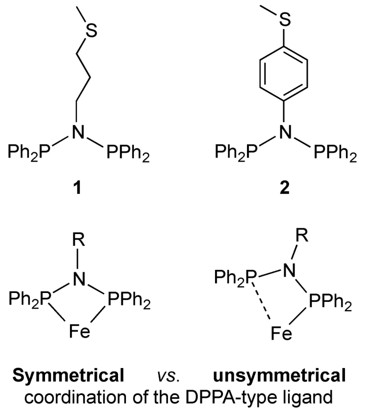

thioether function, which can act as an intra- or intermolecular donor toward a metal center or be used to deposit/anchor complexes on metal surfaces, and (ii) the possibility to evaluate the differences of reactivity induced by a change of the linker that connects the PNP moiety and the thioether donor group, for example, when going from a flexible propyl to a rigid phenyl. Previous studies have shown that (i) bis-chelated dicationic Pd(II) complexes with ligands **1** and **2** could be used to assess molecular anchoring on Au surfaces (Janus microspheres),[4] (ii) the *N*-functionalization influences the behavior of Ni(II) complexes containing such tritopic *P,P,S* ligands in catalytic ethylene oligomerization,[6a] and (iii) a combination of dicationic Ni(II) complexes containing two chelating ligands **1** or **2** and Zn metal allows the activation of both C_{sp3}−Cl bonds of CH_2Cl_2 under mild conditions and affords mixed phosphine, phosphonium ylide species.[10]

Further indications that subtle changes in ligand design can strongly affect the nature of the resulting coordination complexes were also provided by the reactions between $FeCl_2$ and ligand **1** or **2** (1:1 molar ratio) since they led, under strictly similar reaction conditions, to an infinite coordination polymer or a dinuclear complex, respectively.[11] It was concluded that electronic factors accounted for the unusual unsymmetrical chelation of the iron center (Chart 1, bottom), raising the question of a possible lability of phosphorus donors in solution, which is relevant to catalyst behavior. Whereas studies on the coordination chemistry of DPPA-type ligands have mostly focused on metals of groups 6, 10, and 11, Ru and Rh,[5,12] those on Fe and Co remain scarce, although these earth-abundant metals are of considerable current interest and display versatile coordination spheres (coordination numbers and geometries) associated with diverse chemical and physical properties.[13] One should of course remember that the structures of the metal complexes in solution and in the solid state may not be identical, which justifies the use of various complementary methods for their investigation.

Following these observations and recent findings on the magnetic properties of polynuclear Co(II) complexes,[14] we investigated the coordination chemistry of ligands **1** and **2** in cobalt complexes, a metal not much represented in the DPPA-type chemistry landscape. Unexpectedly, dinuclear structures were obtained, as established by X-ray diffraction in the case of the zwitterionic complex $[CoCl_2(\mathbf{1})]_2$ (**3**), which contains one CoCl moiety bis-chelated by two ligands **1** and one $CoCl_3$ fragment coordinated by the S atom of a thioether function. In the absence of X-ray diffraction data for $[CoCl_2(\mathbf{2})]_2$ (**4**) and in order to better understand its occurrence and properties, we compared its spectroscopic features with those of potential constitutive building blocks. This approach was first validated by performing a similar analysis with **3**. The comparisons were based on FT-IR, UV−vis, and EPR spectroscopic data, magnetic measurements, and theoretical calculations.

■ RESULTS AND DISCUSSION

1. Synthesis of the Co(II) Complexes and Solid-State Molecular Structures. To evaluate the influence of the linker that connects the *S*-donor and the *PNP* nitrogen atom of ligands **1** and **2** on the nature of their cobalt(II) complexes, these ligands were initially reacted with an equimolar amount of anhydrous $CoCl_2$ in dichloromethane. In both cases, dark green solutions were obtained and the same workup was applied. After filtration of the reaction mixture, evaporation to dryness of the filtrate, and washing of the residue, a green solid was isolated. Crystallization from a dichloromethane/pentane mixture led to dichroic green/red crystals of complex **3** (ligand **1**) and green polycrystalline $[CoCl_2(\mathbf{2})]_2$ (**4**) (ligand **2**) in 55% and 83% yields, respectively (Scheme 1).

Whereas ^{31}P NMR spectroscopy is commonly used to assess the coordination behavior of *N*-functionalized DPPA-type ligands,[1] this was not possible here owing to the paramagnetic nature of the Co(II) center. The precise determination of the coordination sphere around the metal center thus required X-ray diffraction studies on single crystals, complemented by physical and theoretical investigations (see below). While the molecular structure of complex **3** in $\mathbf{3}\cdot 2CH_2Cl_2$ was unambiguously established by X-ray diffraction studies (Figure

Scheme 1. Reactions of Ligands 1 and 2 with Anhydrous $CoCl_2$[a]

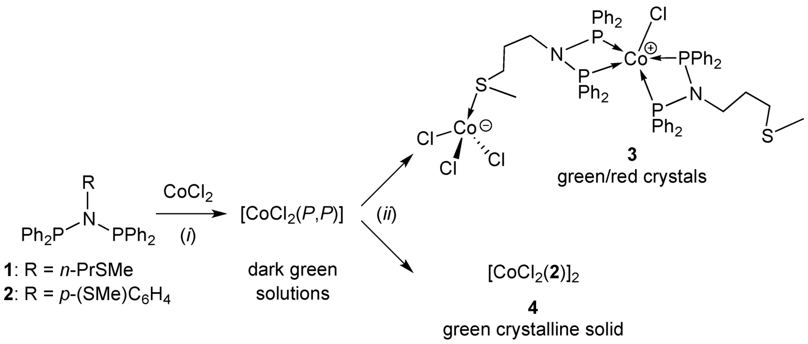

[a]Conditions: (*i*) CH_2Cl_2, room temperature, 12 h, (*ii*) crystallization from CH_2Cl_2/pentane.

DOI: 10.1021/acs.inorgchem.5b02889

1), no suitable single crystals could be obtained for complex **4** despite many attempts.

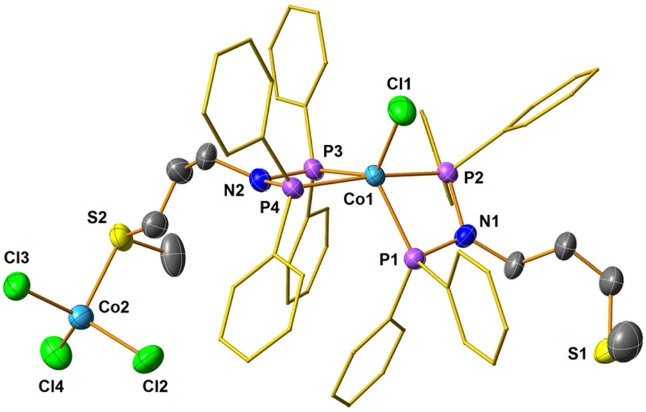

Figure 1. View of the molecular structure of the zwitterionic complex **3** in **3**·$2CH_2Cl_2$. Solvent molecules and hydrogen atoms were omitted for clarity. Ellipsoids are represented at the 50% probability level. Selected bond lengths and angles are reported in Table 1.

The dinuclear complex **3** contains one CoCl moiety bis-chelated by two ligands **1** and one $CoCl_3$ fragment coordinated by the S atom of one thioether function (Figure 1). The 1:1 ligand/metal molar ratio used in the synthesis is retained in the structure of the complex, as confirmed by the elemental analysis on ground and dried crystals (see Experimental Section). To the best of our knowledge, there are only 3 examples of structurally characterized cobalt complexes containing one or two *N*-substituted DPPA-type ligands, and none of them exhibits the observed $[CoCl(P,P)_2]$ or the anticipated $[CoCl_2(P,P)]$ motif (Figure S25 in ESI).[15] Panda et al. reported the formation of a mixed-valent dinuclear complex $[Co^{II}Cl_2(P,P)_2]/[Co^{III}Cl_3(NH_2\text{-}R)]$, resulting from the reaction of a *N*-aryl DPPA-type ligand with $CoCl_2$.[15a] The $[CoCl_3(RSR')]$ motif is also rare, with only three structures available in the CSD database;[16] two of them are $Co^{II}(\mu_2\text{-}Cl)$ dinuclear complexes, and one contains a Co^{III} center (Figure S26 in ESI). The two chemically different Co centers in **3** exhibit different coordination geometries and are formally part of a cationic (Co1) and an anionic fragment (Co2). The pentacoordination around Co1 corresponds to a slightly distorted trigonal bipyramidal geometry, with P1, P3, and Cl1 being coplanar and the apical positions being occupied by P2 and P4. The longest basal P–Co bond is P1–Co1 [2.283(2) Å], whereas the Co1–P3 [2.221(2) Å] and Co1–Cl [2.232(2) Å] bond lengths are similar; likewise, those between the metal center and the apical ligands are similar [Co1–P2 2.248(2) Å and Co1–P4 2.233(2) Å)]. The distortion away from a regular trigonal bipyramidal geometry, as quantified by a continuous symmetry measure $S(D_{3h}) = 2.11$ (see Table S10 in ESI),[17] is induced by the PNP chelate, with P1–Co1–P2 and P3–Co1–P4 angles of 71.69(6)° and 71.33(7)°, respectively. The second Co center (Co2) is in a distorted tetrahedral coordination environment containing three similarly spaced Cl ligands [Co–Cl bond lengths in the range 2.236(2)–2.246(2) Å], whereas the Co2–S2 bond of 2.396(2) Å is significantly longer, consistent with the larger covalent radius of S vs Cl. The angles involving S2 span a broader range [between Cl3–Co2–S2 97.74(7)° and Cl4–Co2–S2 108.49(8)°] than those involving only chlorides and the cobalt center [between Cl4–Co2–Cl2 112.79(9)° and Cl3–Co2–Cl2 117.92(8)°].

The structure of complex **4** could not be determined by single-crystal X-ray diffraction analysis, but elemental analysis performed on a microcrystalline powder was in agreement with the 1:1 ligand/metal ratio used, as in **3** (see Experimental Section). Interestingly, in the ESI-MS spectra ($MeCN/CH_2Cl_2$ solutions) of **3** and **4**, both the $[M - H - CoCl_4]^+$ (*m*/*z* 1005.1 (**3**) and 1073.1 (**4**)) and the $[M - CoCl_3]^+$ fragments (*m*/*z* 1040.1 (**3**) and 1108.1 (**4**)), were detected as major peaks, however with a 4:1 and 2:1 ratio in intensity, respectively.

We expected to gain more information about the nature of **4** from a comparison of its far-infrared (far-FT-IR) spectrum in the region corresponding to the ν(Co–Cl) vibrations (600–100 cm^{-1}) with that of complex **3**. However, the spectra recorded were not conclusive (see below).

At this stage, two hypotheses concerning the structure of complex **4** could be reasonably envisaged: (i) a structure similar to that of complex **3**, with a CoCl moiety bis-chelated by two ligands **2** and a $CoCl_3$ fragment coordinated by a thioether donor[2a] (Chart 2, left), or (ii) an ion pair with a tetrahedral dicationic bis-chelated Co center associated with a $CoCl_4$ dianion (Chart 2, right). The latter situation, i.e., the formation of a ML_2/MCl_4 (L = chelating ligand) formula isomer of a MCl_2L complex, has been recently observed in a Ni(II) complex supported by the monosulfido ligand **1**·S, in which a dicationic Ni(II) center was bis-chelated by two (*P*,P=*S*) ligands, while a $NiCl_4$ dianion balanced the charge.[18]

Since the molecular structure of **4** was not directly accessible by X-ray crystallography or indirectly by comparison of its spectroscopic data (FT-IR, UV–vis, EPR see below) with those of zwitterion **3**, we targeted the formation of mononuclear complexes/fragments potential building blocks of **4** to access their spectroscopic fingerprints, compare them with those of **4**, and see whether the latter could be analyzed as being the "simple" superposition of those of the constitutive fragments.

First applied to the structurally characterized complex **3** for validation, this strategy led us to synthesize the complex $[CoCl(\mathbf{1})_2]PF_6$ (**5**) containing the anticipated cationic (*P*,*P*)-bis-chelated CoCl unit and the zwitterionic complex $[CoCl_3(H\mathbf{1}')]$ (**6**) ($\mathbf{1}' = NH_2(CH_2)_3SMe$), which displays the anionic S-$CoCl_3$ moiety (Scheme 2).

Complex **5** was obtained in nearly quantitative yield by reaction of anhydrous $CoCl_2$ with ligand **1** in a 1:2 metal/ligand ratio in the presence of excess KPF_6 and was isolated as red

Chart 2. Proposed Zwitterionic (4, left) and Ion Pair (4′, right) Forms for Complex $[CoCl_2(\mathbf{2})]_2$

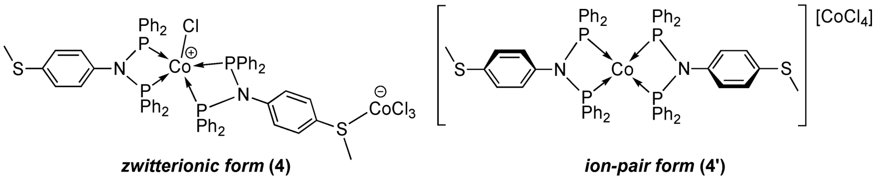

zwitterionic form (**4**)

ion-pair form (**4′**)

Scheme 2. Synthesis and Structure of the Zwitterionic Complex 3 and Its Representative [CoCl(1)$_2$]PF$_6$ (5) and [CoCl$_3$(H1′)] (6) "Fragments"

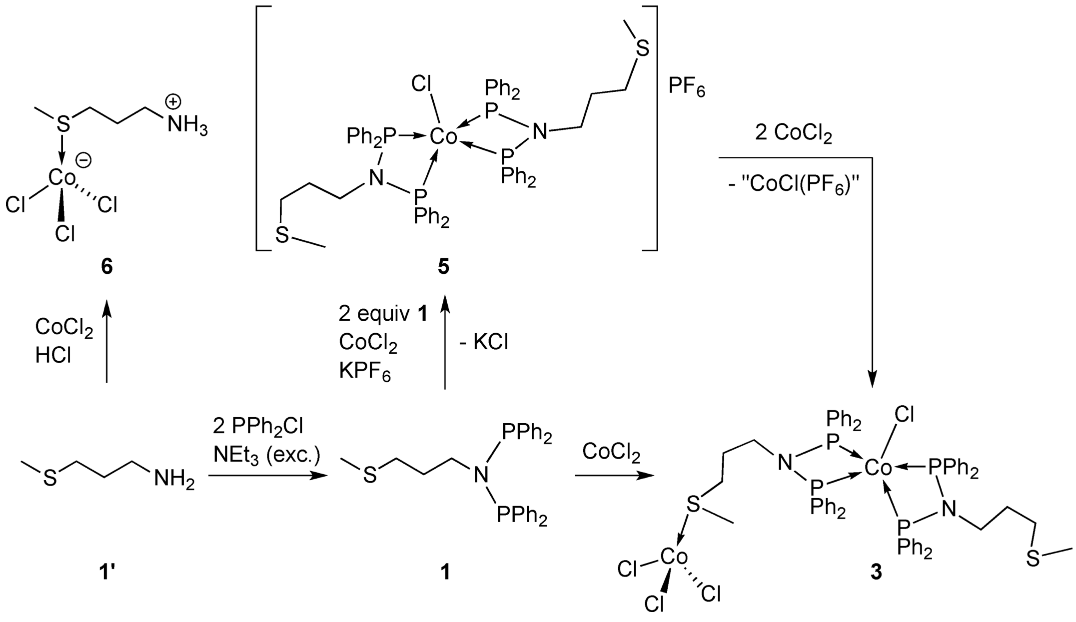

crystals. Elemental and MS analyses were in agreement with its crystal structure (Figure 2). The structural parameters around the Co center (Co1) are, as expected, very close to those found for Co1 in complex 3·2CH$_2$Cl$_2$ (selected bond lengths and angles are reported in Table 1). The cobalt(II) center is bis-chelated by two ligands 1 and adopts again a distorted trigonal bipyramidal coordination geometry, as quantified by a S(D_{3h}) = 2.47 measure (Table S10), in which the base contains two phosphorus atoms from different ligands (P1, P3), with Co−P bond lengths of 2.240(1) (P1) and 2.264(1) Å (P3) and one chlorine [Co−Cl1 2.227(1) Å], while two phosphorus donors occupy the apical positions and exhibit Co−P bond lengths close to those for the basal ones [Co1−P2 and Co1−P4 2.239(2) and 2.241(2) Å, respectively]. The cationic charge on the cobalt center is balanced by an isolated PF$_6$ anion. The major peak recorded in the ESI-MS spectrum of complex **5** was found at m/z 1040.2 and attributed to the [M − PF$_6$]$^+$ fragment. The far-FT-IR spectrum of **5** was also recorded and compared with that of the zwitterionic complex **3** (see below).

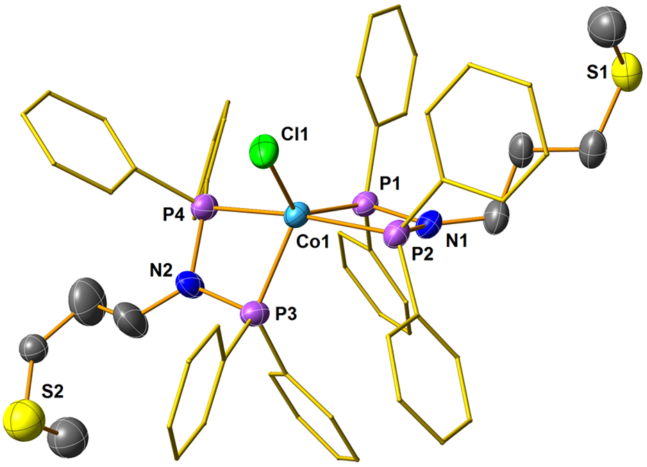

Figure 2. View of the molecular structure of the cationic complex in **5**·CH$_2$Cl$_2$. Counter ion, solvent molecule, and hydrogen atoms omitted for clarity. Ellipsoids are represented at the 50% probability level. Selected bond lengths and angles are reported in Table 1.

Gratifyingly, the reaction of **5** with 2 equiv of anhydrous CoCl$_2$ also afforded the zwitterionic complex **3** with concomitant formation of "CoClPF$_6$" (not isolated).

The complex [CoCl$_3$(H**1′**)] (**6**) (**1′** = NH$_2$(CH$_2$)$_3$SMe) was obtained stepwise by (i) addition of a HCl aqueous solution to a CH$_2$Cl$_2$ solution of 3-(methylthio)propylamine **1′**, the amine precursor to ligand **1**, leading to the corresponding ammonium chloride (not isolated), and (ii) addition of CoCl$_2$, which captured a chloride ion and completed its coordination sphere with the thioether donor function of the ligand. The structure of the zwitterionic complex **6** was confirmed by single-crystal X-ray diffraction studies and, as expected, revealed structural parameters very similar to those of Co2 in complex **3**·2CH$_2$Cl$_2$ (Figure 3 and Table 1). The anionic cobalt(II) center has a distorted tetrahedral coordination geometry with Co−Cl bond lengths ranging from 2.233(8) (Cl2) to 2.264(8) Å (Cl3), close to those found in **3**, and a Co1−S1 bond of 2.365(9) Å, shorter than in complex **3** [Co2−S2 2.396(2) Å].

Complex **6** was also characterized by EA, ESI-MS (major peak m/z 234.9 attributed to [M − Cl]$^+$), and FT-IR spectroscopy (see below).

Our strategy consisting in the independent synthesis of mononuclear cobalt(II) complexes (**5** and **6**) with ligand **1** relevant to complex **3** being validated, it was applied to complexes based on ligand **2**. We thus prepared and isolated the different moieties (**7** and **8**) related to complex **4** (Scheme 3).

Similarly to complex **5**, the cationic bis(P,P)-chelated complex [CoCl(**2**)$_2$]PF$_6$ (**7**) was synthesized by reaction between anhydrous CoCl$_2$ and ligand **2**, in a 1:2 metal/ligand ratio, in the presence of excess KPF$_6$. Complex **7** was isolated after recrystallization as green crystals and characterized by EA, ESI-MS (m/z 1108.2 [M − PF$_6$]$^+$), and FT-IR spectroscopy. Moreover, its molecular structure was determined in the solid-

Table 1. Selected Bond Lengths (Angstroms) and Angles (degrees) in the Solid-State Structures of $3{\cdot}2CH_2Cl_2$, $5{\cdot}CH_2Cl_2$, 6, 7, and 8

	$3{\cdot}2CH_2Cl_2$	$5{\cdot}CH_2Cl_2$	7
Co1−P1	2.283(2)	2.240(1)	2.232(1)
Co1−P2	2.248(2)	2.239(2)	2.223(1)
Co1−P3	2.221(2)	2.264(1)	2.245(9)
Co1−P4	2.233(2)	2.241(2)	2.223(1)
Co1−Cl1	2.232(2)	2.227(1)	2.224(1)
Co2−S2	2.396(2)		
Co2−Cl2	2.246(2)		
Co2−Cl3	2.236(2)		
Co2−Cl4	2.242(2)		
P1−Co1−P2	71.69(6)	71.65(5)	71.93(3)
P3−Co1−P4	71.33(7)	71.32(5)	72.20(3)
P1−Co1−Cl1	119.5(7)	134.8(6)	127.6(4)
P3−Co1−Cl1	128.0(7)	118.8(6)	123.9(4)
S2−Co2−Cl2	100.4 (7)		
Cl2−Co2−Cl3	117.9 (8)		
P1−N1−P2	102.6(3)	101.7(2)	99.4(2)
P3−N2−P4	99.0(3)	101.7(2)	100.2(2)

	6
Co1−S1	2.365(9)
Co1−Cl1	2.251(8)
Co1−Cl2	2.233(8)
Co1−Cl3	2.264(8)
S1−Co1−Cl1	108.3(3)
S1−Co1−Cl2	114.1(3)
S1−Co1−Cl3	96.6(3)
Cl1−Co1−Cl2	113.5(3)
Cl1−Co1−Cl3	113.0(3)
Cl2−Co1−Cl3	110.3(3)
C1−S1−C4	101.2(2)

	8
Co1−Cl4	2.272(6)
Co1−Cl1	2.271(5)
Co1−Cl2	2.257(6)
Co1−Cl3	2.293(5)
Cl1−Co1−Cl4	105.7(2)
Cl2−Co1−Cl4	110.7(2)
Cl3−Co1−Cl4	106.8(2)
Cl1−Co1−Cl2	115.3(2)
Cl1−Co1−Cl3	108.6(2)
Cl2−Co1−Cl3	109.4(2)
C1−S1−C7	103.0(1)
C8−S2−C14	104.6(1)

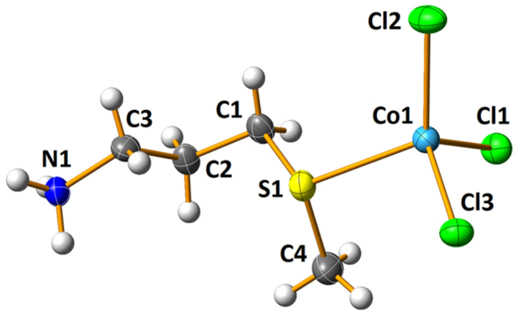

Figure 3. View of the molecular structure of $[CoCl_3(H1')]$ (**6**) (**1′** = $NH_2(CH_2)_3SMe$). Ellipsoids are represented at the 50% probability level. Selected bond lengths and angles are reported in Table 1.

state by X-ray diffraction analysis (Figure 4). As expected, the cationic cobalt(II) center has a distorted trigonal bipyramidal coordination geometry, as quantified by a $S(D_{3h})$ = 2.18 measure (Table S10), in which the base contains two phosphorus atoms from two ligands (P1, P3) and is completed by one chlorine atom (Cl1), while the apical positions are occupied by the two other P atoms (P2, P4) from the chelates. Interestingly, the characteristic structural parameters, i.e., bond lengths and angles around the cationic cobalt center, are very similar to those found in the analogous complex **5** with ligand **1** (Table 1). As was observed for **5**, addition of 2 equiv of anhydrous $CoCl_2$ to a CH_2Cl_2 solution of complex **7** led to the formation of complex **4** (evidenced by FT-IR and EA).

Attempts to synthesize independently the anionic moiety potentially present in the zwitterionic complex **4** by a similar procedure to that used to access the S-$CoCl_3$ fragment of **6** led surprisingly to a different outcome. Reaction of the amine $MeS(p\text{-}C_6H_4)NH_2$ (**2′**), precursor to ligand **2**, with aqueous HCl, followed by treatment with $CoCl_2$, led to an intense blue powder (further identified as complex **8**) along with some unreacted $CoCl_2$. While the analytical results performed on this product were not consistent with the expected $[CoCl_3(H2')]$ formulation, its ESI-MS spectrum only revealed the peak corresponding to the ammonium chloride salt **2′**·HCl. The far-FT-IR spectrum of the isolated compound was also different from that of the zwitterionic complex $[CoCl_3(H1')]$ (**6**) (see below). Fortunately, suitable crystals for X-ray diffraction analysis were obtained and revealed that in the solid state the structure of complex **8** is composed of a $CoCl_4$ dianion and two H2′ ammonium cations (Figure 5). This observation is in accordance with the fact that unreacted $CoCl_2$ was isolated and suggests that an ion-pair formulation for complex **4**, i.e., $[Co(\mathbf{2})_2][CoCl_4]$, could be also reasonably envisaged instead of a zwitterionic structure.

Attempts were made to synthesize trinuclear cobalt(II) complexes in which both thioether functions of ligand **1** or **2** would be coordinated to a $CoCl_2$ or $[CoCl_3]^-$ moiety by reacting (i) complex **3** (or **4**) with 1 equiv $CoCl_2$ or $[HNEt_3][CoCl_3]$ and (ii) complex **5** (or **6**) with 2 equiv $[HNEt_3][CoCl_3]$ (generated in situ), respectively. Unfortunately, these reactions did not lead to the expected compounds, but few crystals of the mixed-valent Co(II)/Co(III) polynuclear complexes $[CoCl_2(\mathbf{1})_2CoCl_3]_n$ (**9**) and $[CoCl_2(\mathbf{2})_2]$-$(H2')[CoCl_4]$ (**10**) (Scheme 4) were isolated, and their crystal structures are shown in the ESI (Figures S27 and S28).

Since a rational synthesis could not be devised nor full analytical data obtained for complexes **9** and **10**, they will not be discussed further. However, we note similarities between the coordination polymer **9** and **3** (the pentacoordinated Co(II) and the tetracoordinated Co(II) centers of **3** being replaced by a hexacoordinated Co(III) and a pentacoordinated Co(II) center, respectively) and between the cationic complexes in **10** and **7** (the pentacoordinated Co(II) center of the latter being replaced by a hexacoordinated Co(III) center).

2. Far-FT-IR and UV−vis Spectroscopic Data. With the aim to validate our approach consisting in the synthesis of molecular synthons (here compounds **5**−**8**) to clarify the structure of an unknown (complex **4**) and more complex architecture (complexes **3** and **4**), we studied their vibrational spectra in the far-infrared region corresponding to the ν(Co−Cl) vibrations and their absorption electronic spectra in solution.

DOI: 10.1021/acs.inorgchem.5b02889
Inorg. Chem. XXXX, XXX, XXX−XXX

Scheme 3. Synthesis and Proposed Structure of Complex 4 and the Relevant "Fragments" $[CoCl(2)_2]PF_6$ (7) and $[H2']_2[CoCl_4]$ (8)

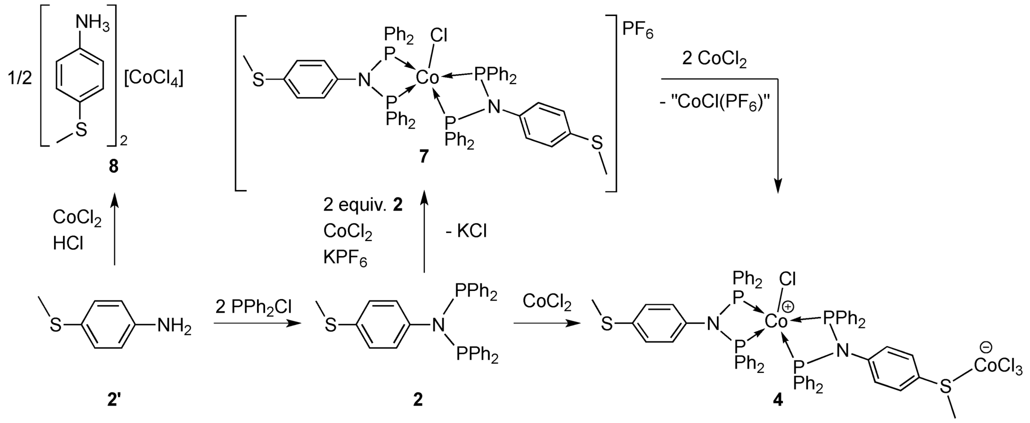

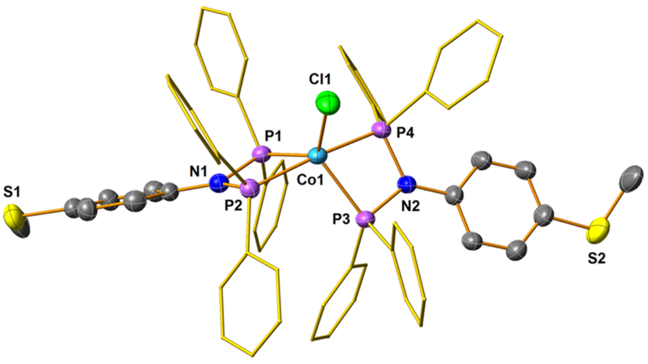

Figure 4. View of the molecular structure of the cationic complex in 7. Counterion and hydrogen atoms omitted for clarity. Ellipsoids are represented at the 50% probability level. Selected bond lengths and angles are reported in Table 1.

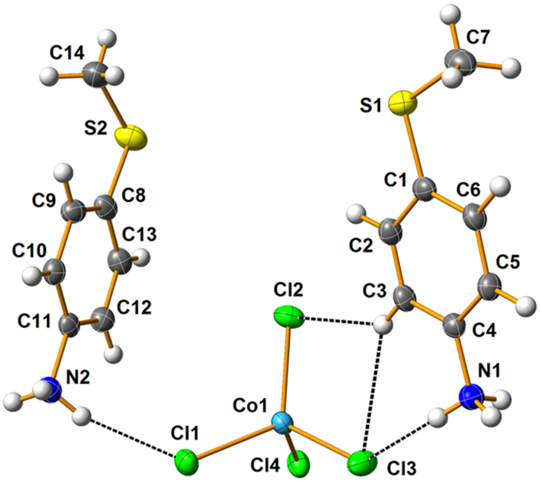

Figure 5. View of the molecular structure of 8. Ellipsoids are represented at the 50% probability level. Selected bond lengths and angles are reported in Table 1.

Scheme 4. Polynuclear Complexes $[CoCl_2(1)_2CoCl_3]_n$ (9) and $[CoCl_2(2)_2](H2')[CoCl_4]$ (10) (see Figures S27 and S28)

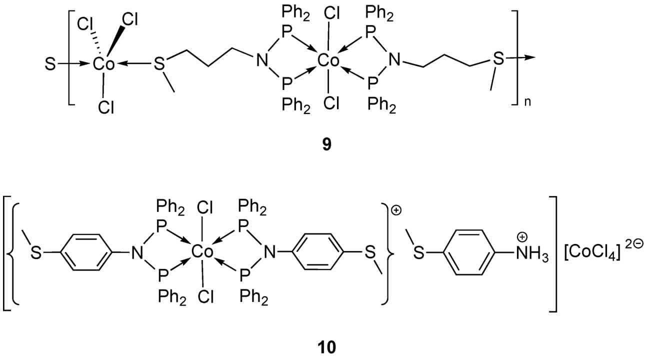

While the far-FT-IR spectrum of complex 3 exhibited four absorptions of medium intensity at ν = 530 (well separated from the other), 510, 490, and 480 cm^{-1} and one intense band at ν = 320 cm^{-1} with weaker shoulders (Figure S1 in ESI), the spectrum of complex 4 exhibited three large and distinct bands at ν = 557, 526, and 495 cm^{-1} and two intense bands at ν = 307 and 296 cm^{-1} with weak shoulders (Figure S5 in ESI). Both compounds also presented weak absorptions in the 430−360 cm^{-1} region. The complexity of these spectra encouraged us to compare the spectrum of each compound with those of their suggested fragments (5 and 6 for 3 and 7 and 8 for 4, Schemes 2 and 3, respectively).

As expected, the far-IR spectra of complexes 5 and 6, when superimposed to that of complex 3, showed significant similarities (Figure 6). The spectrum of 6 exhibits three absorptions at 320, 305, and 289 cm^{-1} assigned to the distorted

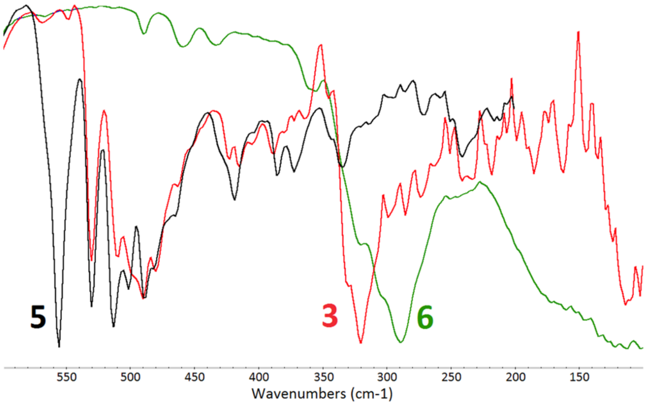

Figure 6. Superimposition of the IR spectra of complexes 3, 5, and 6 in the 600−100 cm^{-1} region.

tetrahedral S-$CoCl_3$ moiety, and their pattern is comparable to that found for **3**, however shifted to lower wavenumbers (Figures S1 (**3**) and S3 (**6**) in ESI). Interestingly, none of these absorption bands was detected in the spectrum of **5**. In contrast, various strong vibration bands between 550 and 480 cm^{-1} are present in both spectra of **3** and **5** (Figures S1 (**3**) and S2 (**5**) in ESI).

A comparison between the far-FT-IR spectra of complexes **4** and **7** also revealed close similarities with four absorptions at 554, 526, 495, and 423 cm^{-1} for **4** and 556, 526, 492, and 425 cm^{-1} for **7** (Figures 7, and S5 (**4**) and S6 (**7**) in ESI). However, complex **4** exhibits strong and broad absorption bands centered at 295 cm^{-1}, in contrast to **7**. The spectrum of **8** exhibits three very intense, well-separated absorptions at 322, 294, and 272 cm^{-1} (Figure S7 in ESI, the splitting of the T mode expected for a perfectly tetrahedral $[CoC1_4]^{2-}$ dianion results from a lowering of the local symmetry). Compared with those of **4**, the different shape of the bands could be due to intermolecular nonclassical H−Cl bonds or packing effects. In this spectral region, the spectrum of **6** ($CoCl_3$ fragment) also exhibits broad and poorly resolved absorption bands, with the most intense at 289 cm^{-1}. Therefore, it is not possible to unambiguously conclude on the basis of FT-IR data about the presence of a $CoCl_4$ or a $CoCl_3$ fragment in complex **4**.

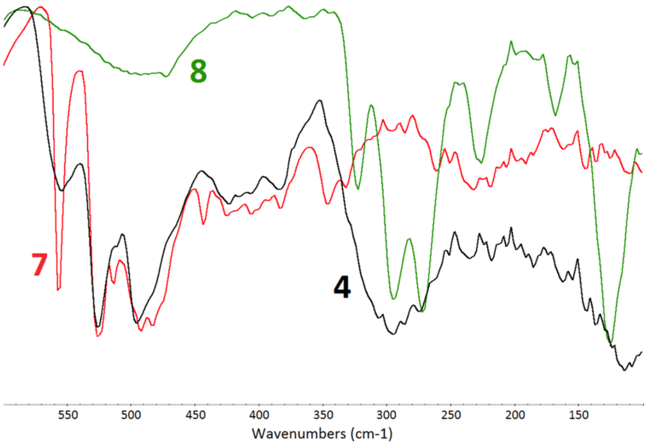

Figure 7. Superimposition of the IR spectra of complexes **4**, **7**, and **8** in the 600−100 cm^{-1} region.

We then recorded the UV−vis spectra of all the isolated compounds with ligand **1**. The spectra of the dinuclear zwitterionic complex **3** and of the mononuclear cationic complex **5** (both in $CHCl_3$) presented the same characteristic absorption bands at 350, 375, and 470 nm (Figure 8). However, the spectrum of **3** exhibits a further absorption at 585 nm (in $CHCl_3$ and THF) that is not present in the spectrum of **5**, but a similar absorption (λ 590 nm) was recorded in the spectrum of the zwitterion **6** (in THF because of insolubility in $CHCl_3$, Figure 8 insert), which is characteristic of a $^4T_1(P) \leftarrow {}^4A_2$ transition split by spin−orbit coupling.[19] These observations led us to conclude that the spectrum of **3** can be viewed as the superposition of the spectra of complexes **5** ($Co^+Cl(P,P)_2$ fragment) and **6** (SCo^-Cl_3 fragment), and this encouraged us to study further the UV−vis spectra of complexes **7** and **8**, potential mononuclear building blocks of complex **4**.

Interestingly, in the case of the complexes supported by ligand **2**, we initially observed that **4** exhibited a different spectrum in $CHCl_3$ and in THF, in contrast to **3**, which has similar spectra in both solvents. While the spectrum of **4** in $CHCl_3$ closely resembles those of complexes **7** (in $CHCl_3$) and **3** (Figure S9 in ESI), with a very intense absorption band below 330 nm, a large shoulder until 375 nm, and two of lower intensity at 460 and 690 nm, its spectrum in THF is clearly different (Figure 9). The strong absorptions below 330 nm remain present in the spectrum of **4** in THF, but instead of a shoulder, there is a strong, sharp absorption at 370 nm. The most important differences are found at higher wavelengths, since the absorption at 460 nm for **4** and **7** in $CHCl_3$ is not present in the spectrum of **4** in THF, while an absorption band of low intensity appeared at 585 nm, which is also present in the spectrum of complex **8** in THF (Figure 9 insert). Noteworthy, the UV−vis spectrum reported for the

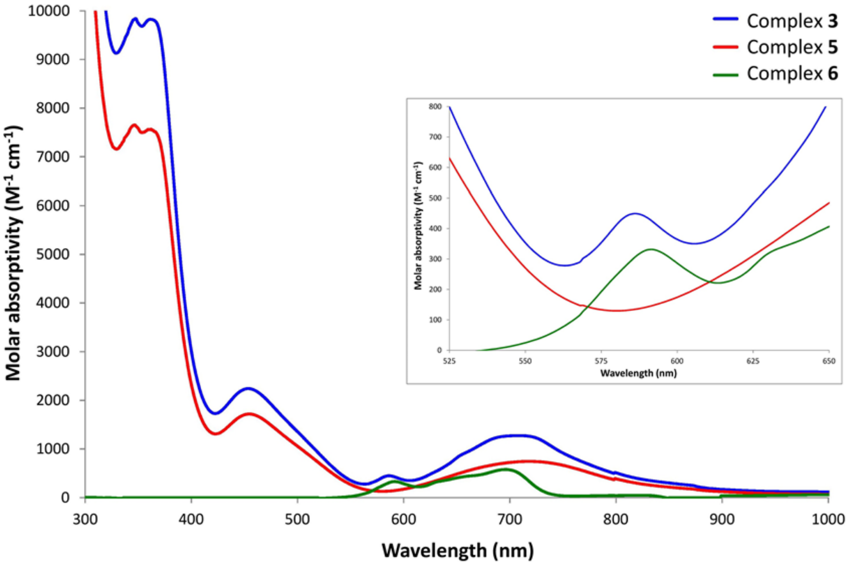

Figure 8. UV−vis spectra of compounds **3** (2×10^{-4} M in $CHCl_3$), **5** (4×10^{-4} M in $CHCl_3$), and **6** (3×10^{-4} M in THF) and zoom in the 525−650 nm region, highlighting the fact that the spectrum of the dinuclear zwitterionic complex **3** is nearly the sum of those from the mononuclear complexes **5** and **6**.

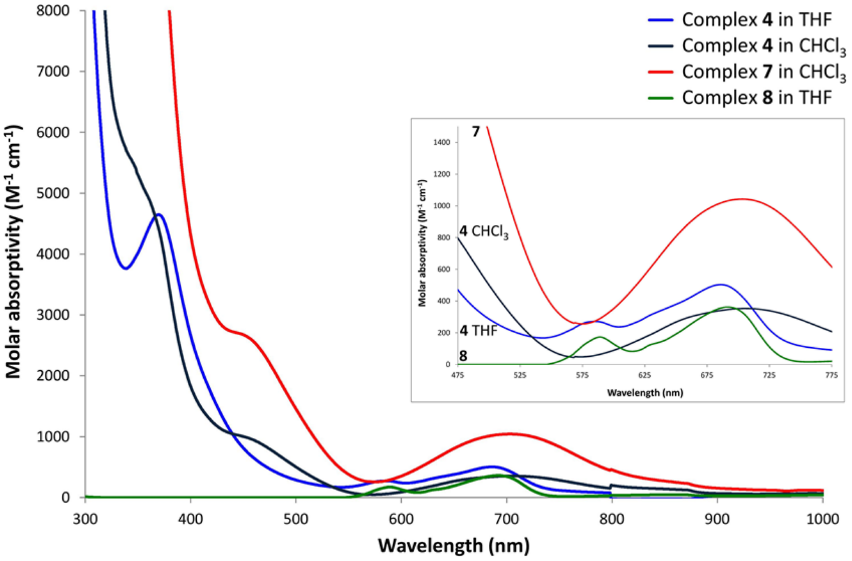

Figure 9. UV−vis spectra of compounds **4** (4×10^{-4} M in THF and 2×10^{-4} M in $CHCl_3$), **7** (2×10^{-4} M in $CHCl_3$), and **8** (4×10^{-4} M in THF) and zoom in the 475−775 nm region.

$[CoCl_3(THF)]^-$ anion exhibits the similar two characteristic absorption bands at 587 and 693 cm^{-1} (vs 585 and 690 cm^{-1} for **4** and **8**), which were ascribed to the d−d transition from the ground state $^4A_2$ to the $^4T_1(P)$ state.[20] Altogether, the fact that complex **8** exhibits different spectra in $CHCl_3$ and THF and that the spectra of complexes **4** and **8** (in THF) present exactly the same pattern in the 550−750 nm region as the $[CoCl_3(THF)]^-$ anion is in favor of a zwitterionic form (vs ion pair, Chart 2) for the dinuclear complex **4**, whose weakly coordinated $CoCl_3$ fragment would be displaced by THF. The UV−vis spectrum of a pseudotetrahedral $[CoCl(\mu\text{-}Cl)(Me_2\text{-}cAAC)]_2$ complex, formally presenting a $LCoCl_3$ fragment, also exhibits a similar pattern, with two strong absorption bands around 580 and 650 cm^{-1}.[21] The spectra of complexes **4** and **8** in THF present exactly the same pattern

The UV−vis studies revealed clearly that the spectrum of the bis-cobalt complex **3** combines the different absorption bands observed for its constitutive mononuclear fragments **5** and **6**, independently of the solvent used. With complexes supported by ligand **2**, we observed that the spectrum recorded for complex **4** is solvent dependent and different from that of complex **3**, while both couples of complexes **5**/**7** and **6**/**8** exhibit the same characteristic absorptions (Figures S9−11 in ESI). These elements do not allow us to conclude on the exact structure of complex **4**: in a noncoordinating solvent, such as chloroform, it behaves like the cationic bis-chelate $[Co^+Cl(P,P)_2]$ complex **7**, while in coordinating THF, it presents undoubtedly the absorptions recorded for complex **8**.

3. EPR Measurements. The X-band EPR spectra of powder samples of complexes **5** and **7** recorded at 5 K are shown in Figure 10, together with their simulations. As reported in the literature, five-coordinate low-spin (LS) cobalt(II) complexes have been found with soft phosphorus donor ligands.[22] The fit parameters are consistent with a trigonal bipyramidal structure (Table 2).[23] A low-spin (LS) Co(II) $S = 1/2$ doublet is suggested to have weaker anisotropy than the corresponding $S = 3/2$ high-spin (HS) species. Moreover, pulsed EPR indicates longer relaxation times, which are compatible with the usually well-separated energy levels encountered for the LS state.[24] The spectral width is mostly due to the hyperfine interactions with the ^{59}Co nucleus ($I = 7/2$), and the overall signal shape is well reproduced (Table 2).

The X-band EPR spectra of powders of **6** and **8** recorded at 5 K (Figure 10) correspond to Co(II) in a HS quartet spin state. This is usually recognized by poorly resolved resonances, broadened by a combination of large g anisotropy, sizable spin−orbit couplings, and admixture of excited state character into the magnetic ground state.[25] Two strategies may be considered to obtain visually satisfactory simulations of HS Co(II) EPR spectra. Both rely on an effective $S = 1/2$ ground state. The positions of the resonances are then matched either by considering an axial g tensor, hence introducing rhombicity of the zero-field slitting (ZFS),[26] or by considering an axial ZFS and by tuning the anisotropy of the g tensor.[27] It is worth mentioning that mathematically one can often achieve a similarly satisfying visual simulation by using a $M_S = 3/2$ ground state and varying the rhombicity in both g and ZFS, although this provides a wholly indeterminate set of solutions. It is noteworthy that the EPR signal extends well beyond the $g = 2$ region at low temperature, so that more transitions than expected may be observed.[28] In many instances, these "additional" lines appear at fields above 0.5 T, so that partly out-of-range transitions may induce artifacts into the simulations. Simulations of the spectra for **6** and **8** (Table 3) are proposed, while we are fully aware of all these difficulties. These simulations will serve as references for the spectral simulation of the bis-Co complexes described hereafter. The narrower peak-to-peak line width in the signal of **8** may express an isotropic tetrahedral surrounding of the Co nucleus in a $CoCl_4$ environment, while it was anisotropic tetrahedral in **6** ($CoCl_3S$).

The X-band EPR spectra of the powder samples of complexes **3** and **4** show both the LS and the HS features (Figures S12 and 10, respectively) with $g_{eff}(HS) = 5.83$ and $g_{eff}(LS) = 2.17$ for **3** and $g_{eff}(HS) = 5.24$ and $g_{eff}(LS) = 2.11$ for **4**. The anisotropic EPR spectral parameters deduced from simulations are summarized in Table 4.

Numerical simulations satisfactorily accounted for a 1:1 ratio of LS and HS species for the binuclear species. Unfortunately, grain size effects were observed for a polycrystalline powder of

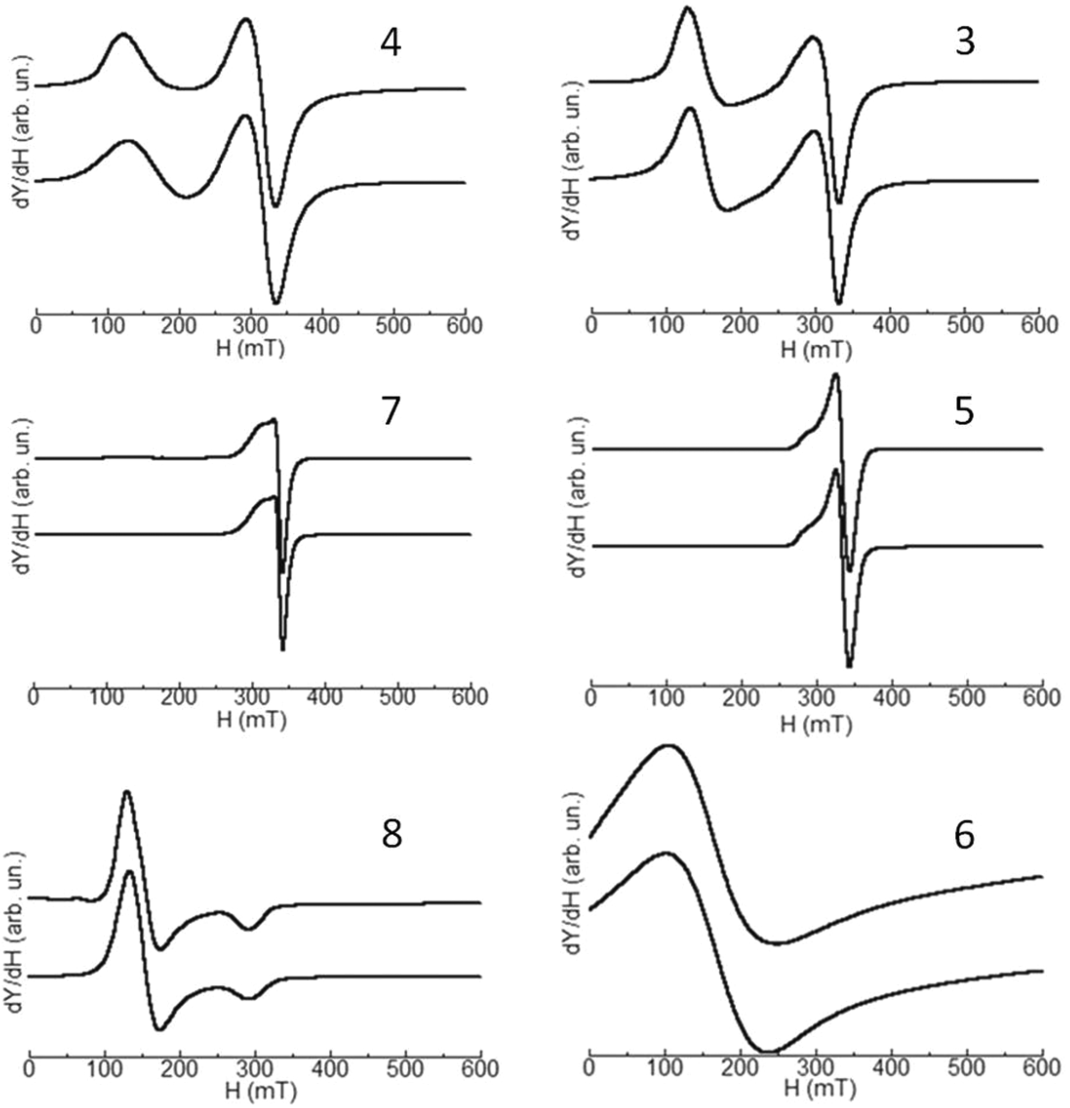

Figure 10. EPR spectra of powder samples of complexes **4**−**8** and of a frozen solution of complex **3** recorded at 5 K: experimental (upper trace) and simulation (lower trace).

Table 2. *g*-Tensor and Hyperfine Tensor Components (hfcc's, A) Deduced by Numerical Simulations of the EPR Spectra of Powder Samples of 5 and 7 recorded at 5 K

	S	g_1	g_2	g_3	A_1 (MHz)	A_2 (MHz)	A_3 (MHz)	lwpp (mT)[a]
7	1/2	2.057		2.288	19		120	5.5 G+L
5	1/2	2.040	2.087	2.350	19	19	140	3.5 G+L

[a] lwpp corresponds to the peak-to-peak line width of the EPR signal with Gaussian (G) and Lorentzian (L) line shape broadening.

Table 3. EPR Parameters Deduced by Numerical Simulations of the EPR Spectra of Powder Samples of 6 and 8

	S	$g_\perp$	$g_\parallel$	ZFS *D* (cm^{-1})	lwpp (mT)[a]
8	3/2	2.240	2.340	>1.5	18 G+L
6	3/2	2.033	2.120	>1.5	65 G+L

[a] lwpp corresponds to the peak-to-peak line width of the EPR signal for Gaussian (G) and Lorentzian (L) line shape broadening.

3, which resulted in an orientation-dependent EPR signal. Although the low-spin region of polycrystalline **3** clearly shows the hyperfine interaction with the *I* = 7/2 ^{59}Co (Figure S12 in ESI), grain size effects prevent a proper assessment of the LS Co hfcc. We did not try to attenuate these effects upon finer grinding, being more concerned with the sample stability (structural and chemical). To remove the underlying ambiguity, we studied sample **3** in frozen solution (Figure 10). This study actually demonstrated the similarity of the LS Co EPR signals for complexes **3** and **6**. EPR studies cannot firmly conclude the possible magnetic exchange between the two Co centers. Accounting for the estimation of such exchange coupling from SQUID measurements (see below), the main conclusion is that the two remote Co magnetic centers are very weakly correlated ($J < 1$ cm^{-1}). At the energy scale of EPR, this is always within the strong exchange limit with $J \gg A$.

4. Magnetic Measurements. We confronted the EPR results with the magnetic data on polycrystalline samples.

DOI: 10.1021/acs.inorgchem.5b02889
Inorg. Chem. XXXX, XXX, XXX−XXX

Table 4. EPR Parameters Deduced from Simulations of the Experimental Spectra of a Frozen Solution of 3 and of a Polycrystalline Powder 4 Recorded at 5 K

	$S = 1/2$						$S = 3/2$				
	$g_1 = g_2$	g_3	$A_1 = A_2$ (MHz)	A_3 (MHz)	lwpp (mT)[a]	%	$g_\perp$	$g_\parallel$	D (cm^{-1})	lwpp (mT)[a]	%
4	2.057	2.288	19	120	31 L	54	2.240	2.340	>1.5	58 L	46
3	2.058	2.410	50	180	25 G+L	50	2.300	2.433	>1.5	48 G+L	50

[a] lwpp corresponds to the peak-to-peak line width of the EPR signal with Gaussian (G) and Lorentzian (L) line shape broadening.

Measurements were performed over the 2−300 K range under 1 or 10 kOe. Figure 11 illustrates the evolution of the $\chi_M T$ product with temperature for **5** and **7**. Compound **5** shows Curie behavior above 20 K, with a Curie value of 0.482(1) cm^3·K·mol^{-1}, while compound **7** shows Curie−Weiss behavior with 0.5663(3) cm^3·K·mol^{-1} and −1.7(1) K (Figure S13 in ESI). Only a slight decrease of the $\chi_M T$ products is observed at low temperatures, in agreement with the low Weiss temperatures, showing that the Co(II) ions are mostly uncorrelated. Isothermal magnetizations tend toward saturation values close to 1 μ_B (Figure S14 in ESI), thus supporting a low-spin $S = 1/2$ ground state. Curves at 5 and 8 K are superimposed on the Brillouin curve for $g = 2.119(1)$ and 2.345(1) for compounds **5** and **7**, respectively. Compounds **5** and **7** show distorted trigonal bipyramidal CoP_4Cl coordination geometries with C_2 symmetry at most. For low-spin Co(II) in *TBPY*-ML_5 geometry, the resulting $^2E'$ ground state is expected to have its orbital momentum quenched but with a Landé g value quite above the free electron value by spin−orbit mixing. Indeed, the effective g values found for compounds **5** and **7**, either from isothermal magnetizations or the Curie parameter (2.267(5) and 2.457(1), respectively) are in the range found by EPR for these compounds and for other low-spin $Co^{II}P_4Cl$ complexes.[22,23,29] Intriguingly, isothermal magnetizations at 1.8 K deviate significantly from the Brillouin curve and cannot be fitted with another Brillouin with reasonable values, which may be symptomatic of the onset of some intermolecular magnetic interactions between Co(II) centers that may not show zero-field splitting but are expected to have strongly anisotropic g tensors.

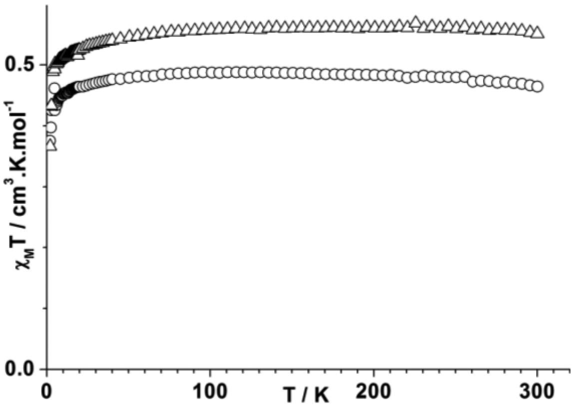

Figure 11. Variation of the $\chi_M T$ product with temperature measured under 10 kOe for compounds **5** (circles) and **7** (triangles).

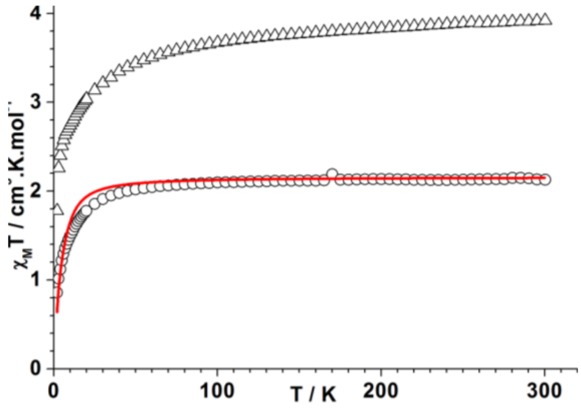

Figure 12. Variation of the $\chi_M T$ product with temperature measured under 1 kOe for compounds **6** (circles) and **8** (triangles), with the simulated curve (red line), for $2S = 3/2$ spins in AF interaction, with $g = 2.147$, $J = -0.4$ cm^{-1}, and $D = +7$ cm^{-1}.

Figure 12 shows the evolution of the $\chi_M T$ product with temperature for **6** and **8**. For both compounds, temperature-independent paramagnetic (TIP) contributions have to be taken into account, a common feature for tetrahedral d^7 Co(II) compounds,[30] with a reasonable TIP value of 450 × 10^{-6} cm^3·mol^{-1} for compound **6**. The latter shows straightforward Curie−Weiss behavior above 50 K, with parameter values of 2.161(2) cm^3·K·mol^{-1} and −3.0(3) K (Figure S15 in ESI), in agreement with largely uncorrelated tetrahedral Co(II) ions in a $^4A_2$ ground state,[31−35] with a spin-only Landé factor g = 2.147(2), significantly larger than the free-electron value. The latter and the high TIP values are expected because of the mixing of the ground state with the low-lying $^4T_2$ state issued from the same ^4F atomic term.[36] Below 50 K, a significant decrease of the $\chi_M T$ product is observed down to 2 K, in agreement with the observed negative Curie−Weiss temperature. Typical nesting behavior is observed in low-temperature isothermal magnetization measurements (Figure S16 in ESI), showing the presence of antiferromagnetic interactions or/and single-ion magnetic anisotropy. Simulations taking into account only single-ion anisotropy proved unsatisfactory to simulate the magnetic behavior observed, all the more so since rhombicity on g and/or the zero-field splitting cannot be reliably extracted from a powder measurement. The crystalline structure shows close contacts between chlorine and cobalt atoms of neighboring complexes, forming effectively pairs of complexes in the structure (Figure S17 in ESI). Using a simple dinuclear model with single-ion anisotropy allows for an acceptable simulation of both $\chi_M T$ and isothermal magnetization curves with the following parameters: $g = 2.147$, $J = -0.4$ cm^{-1}, $D = +7$ cm^{-1}.[37] The interaction parameter agrees with the −0.8 cm^{-1} value deduced from the Curie−Weiss temperature using the mean-field approach.[38] Easy-axis single-ion anisotropies ($D < 0$) led to a worse agreement at low temperature for the $\chi_M T$ curve. The resulting effective g factor value is above the average value of 2.062 found by EPR on a powder sample of **8**. Some discrepancy between single-ion anisotropy values had to be expected given the inherent uncertainty for their determination from powder values.

For compound **8** (Figure 12), even with a strong TIP contribution of 600 × 10^{-6} $cm^3 \cdot mol^{-1}$, as observed in other salts containing a tetrahedral $CoCl_4^{2-}$ anion,[30,36] the $\chi_M T$ value still increases at high temperatures. A TIP value of 1500 × 10^{-6} $cm^3 \cdot mol^{-1}$ would be required to account for the high-temperature behavior, a value that would imply a $^4T_2$ excited state lying at unphysical low energy.[39] Nevertheless, a Curie–Weiss law gives a satisfactory fit above 50 K (Figure S15 in ESI), with values of 4.04 $cm^3 \cdot K \cdot mol^{-1}$ and −10.1 K, depending on the TIP contribution used. These values support again tetrahedral Co(II) ions with a $^4A_2$ ground state but with an unusually high spin-only Landé factor g = 2.9. The low-temperature behavior parallels that observed for compound **6** (Figure 12), with no maximum observable at low temperature on the susceptibility curve but with an isothermal magnetization that does not seem to be close to saturation even at 1.8 K and 70 kOe (Figure S16 in ESI). Close examination of the crystal packing of **8** shows that the $CoCl_4^{2-}$ ions form layers parallel to the *ac* plane, which are separated along the *b* axis by the ammonium moieties (Figure S18 in ESI). The arrangement of the anions within the layers is close to a 2D honeycomb lattice, with close Cl···Cl contacts of about 4 Å. The anomalous magnetic behavior observed may thus be accounted for by correlation effects within those layers between the strongly anisotropic tetrahedral Co(II).[40] Its correct modeling would require further anisotropic measurements on single crystals that are outside the scope of this study.

Figure 13 reports the $\chi_M T$ product evolution with temperature for **3** and **4**. It is readily seen that both compounds show very similar characteristics with Curie–Weiss behavior above 20 K (Figure S19 in ESI) and parameters of 3.408(3) $cm^3 \cdot K \cdot mol^{-1}$ and −4.1(2) K and 3.147(2) $cm^3 \cdot K \cdot mol^{-1}$ and −3.0(1) K, respectively. For both compounds, TIP contributions were taken into account with a reasonable value of 350 × 10^{-6} $cm^3 \cdot mol^{-1}$ for **4**, while **3** showed some slight contamination with ferromagnetic impurities, which could not be deconvoluted from the TIP contribution.

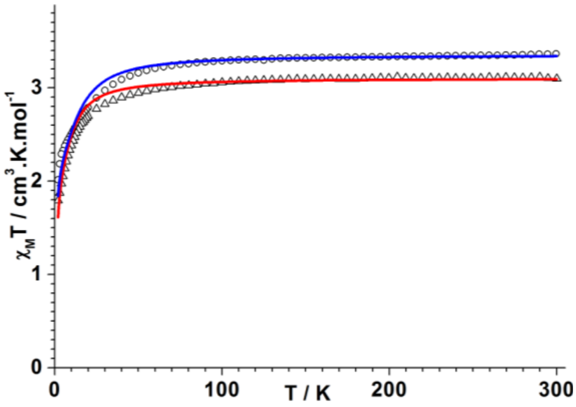

Figure 13. Variation of the $\chi_M T$ product with temperature measured under 1 kOe for compounds **3** (black circles) and **4** (black triangles), and simulated curves (blue and red curves, respectively) for the interacting {1/2;3/2} spin system (see text for parameters).

As indicated above, only for compound **3** is the solid-state structure clearly established, and one could anticipate magnetic properties for **3** close to the sum of those of compounds **5** and **6**. A comparison of the respective $\chi_M T$ products readily shows that although this is the case, in agreement with one low-spin Co(II) in trigonal bipyramidal coordination environment and one high-spin Co(II) with tetrahedral coordination, the single-ion properties vary somewhat, in agreement with the differences seen in the powder EPR spectra of compounds **3**, **5**, and **6**. For **4**, the $\chi_M T$ value at high temperature of 3.1 $cm^3 \cdot K \cdot mol^{-1}$ is quite close to the sum of the corresponding values for compounds **7** and **6** at 2.7 $cm^3 \cdot K \cdot mol^{-1}$, indicating that here also the preferred formulation would be one low-spin Co(II) with trigonal bipyramidal coordination and one high-spin Co(II) with tetrahedral coordination.

For both compounds a strong decrease of the $\chi_M T$ product is observed below 50 K but without any corresponding peak in the susceptibility curve, which indicates that any antiferromagnetic interaction is of low magnitude. Indeed, the structure of compound **3** does not evidence obvious interaction pathways. The decrease observed is thus caused mainly by the zero-field splitting of the $^4A_2$ ground state of the tetrahedrally coordinated Co(II) ions. Though the problem is largely overparametrized, considering axially anisotropic g tensors for both Co(II) ions, the zero-field splitting, and a small intramolecular interaction between both Co(II) ions, reasonable sets of parameters can be found[41] that simulate the overall behavior of both $\chi_M T$ and isothermal magnetization curves (Figures 13 and S20–S21 in ESI). We used the g factors found by EPR for the pentacoordinated low-spin Co(II) and adjusted accordingly the g factor for the tetrahedral Co(II) with an arbitrary ratio $g_\perp / g_\parallel$ fixed at 1.1 for both compounds (this ratio corresponds to that observed by EPR for the high-spin Co(II) in compound **4**). In both cases, using easy-axis zero-field splitting led to worse simulations. The parameters found for compound **3** were $J = -0.3$ cm^{-1}, $S = 1/2$, $g_\perp = 2.135$, and $g_\parallel = 2.402$ and $S = 3/2$, $g_\perp = 2.401$, $g_\parallel = 2.641$, and $D = +15$ cm^{-1} and for compound **4** $J = -0.4$ cm^{-1}, $S = 1/2$, $g_\perp = 2.057$, and $g_\parallel = 2.288$ and $S = 3/2$, $g_\perp = 2.31$, $g_\parallel = 2.541$, and $D = +10$ cm^{-1}.

5. Theoretical DFT Calculations. DFT calculations using the ADF package were performed to determine the geometries and electronic structures of the complexes. Geometry optimizations were performed starting from the X-ray structures. In all cases we found that spin contamination was negligible. For comparison, we first computed mononuclear complexes, viewed as building blocks of the dinuclear complexes. Several conformations for **5** and **7** were considered, but only one has been optimized where the phenyl rings are roughly parallel to the P–N–P planes for **7**, and the positions of the aliphatic chains for **5** are consistent with the X-ray structure. As established experimentally, the Co1 atom in **5** and **7** has an $S = 1/2$ ground state, and therefore, the structures were optimized as a doublet. The calculated geometries for **5** and **7** are similar to the arrangement of the ligands found in the X-ray structures. Relevant computed geometrical parameters are given in Table S2 (ESI) and compared to experimental values. The resulting bond lengths and angles are similar to those found experimentally. The largest deviation concerns the computed Co–P bond distances, which are ca. 0.01–0.1 Å longer than the observed values. The size of the molecules prevented optimization with larger basis sets or higher theory level methods to obtain more accurate values. The coordination sphere around the Co1 atom is distorted trigonal bipyramidal, with $S(D_{3h})$ of 2.25 and 2.32, respectively, quite close to experimental values (2.47 and 2.18) (Table S10). The arrangement of the phenyl moieties and carbon chains is quite well reproduced for **7** and **5**, respectively. As shown in Figure 14b for **5**, the spin density is exclusively centered on the cobalt cation, with very small contributions from the chlorine

DOI: 10.1021/acs.inorgchem.5b02889
Inorg. Chem. XXXX, XXX, XXX−XXX

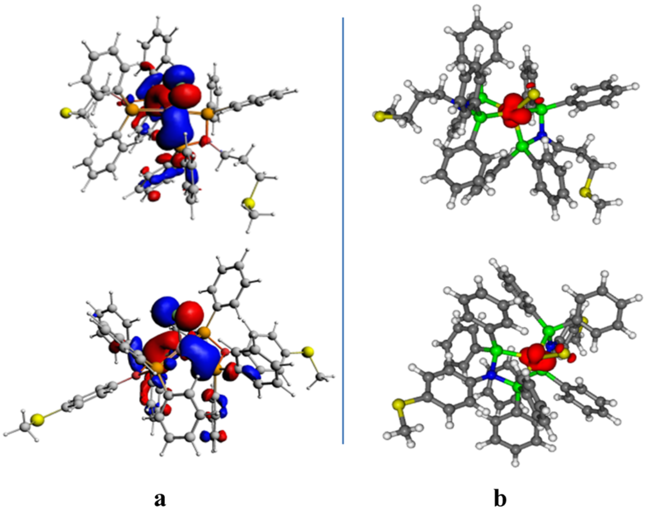

Figure 14. (a) ADF view drawing of the Kohn−Sham singly occupied molecular orbitals (SOMOs) of **5** (top) and **7** (bottom). (b) Spin density plots for **5** (top) and **7** (bottom).

and phosphorus atoms. This spin density is mostly generated by the molecular orbital (SOMO) given in Figure 14a, which is π-antibonding between the Co1 3d orbitals and the chlorine and phosphorus atoms. The situation is almost identical for **7**, with a spin density again mostly localized on the cation. However, the associated SOMO shows some delocalization through the π system of the phenyl rings. Finally, the different substituents on nitrogen have a slight influence on the electronic structure. The EPR parameters were also calculated to evaluate the g tensors through a single point at the B3LYP level of DFT with the ORCA package on the ADF-optimized geometries. The calculated values are listed in Table S3 (ESI). The simulation of the spectra indicated a more rhombic g tensor for **5** than for **7**, which is axial with $g_{\|} > g_{\perp}$. These results are similar to those reported on triphosphine complexes and support the assignment of a trigonal bipyramidal structure with a mixed $d_{x^2-y^2}/d_{xy}$ ground state.[42] This is consistent with the spin density map calculated for the low-spin mononuclear complexes localized on the trigonal equatorial plane. The computed g tensors obtained for both compounds are almost axial and reproduce quite satisfactory the EPR data for **7**. A more important discrepancy is observed for **5** that is attributed to the absence of the surrounding medium, i.e., calculations were performed on the gas phase.

The ground state geometries for **6** and **8** were computed using the experimentally determined $S = 3/2$ ground states. Geometrical parameters calculated for both **6** and **8** indicated a four-coordinated metal center in a tetrahedral environment, which is in good agreement with the experimental data. However, for complex **6**, the calculated distance between Co2 and the nitrogen atoms was divided by approximately two: the zwitterionic structure induces significant Coulombic attraction. The Co2−S and Co2−Cl distances are slightly overestimated and present the same behavior as that described above for **5** and **7**. For **6** and **8**, the metal 3d orbitals contribute to the frontier orbitals with a high participation of the Cl and S atoms. The three highest occupied molecular orbitals (SOMO) for **6** are depicted in Figure S22 (ESI). The EPR spectrum of **8** is dominated by two broad features, whereas for **6** only a very broad signal is observed. The spectral features are similar to the EPR spectra of some substituted tetrahedral complexes reported in the literature.[43] According to calculated tetrahedral geometries and EPR data, the Co(II) ions adopt a high-spin configuration $S = 3/2$. The computed g tensors obtained for both compounds are almost axial and reproduce quite satisfactory the EPR data.

For **3** complex, EPR and SQUID data prompted us to assign a low-spin state $S = 1/2$ to Co1 and a high-spin state $S = 3/2$ to Co2. The computed values for **3** reproduced both environments of Co1 and Co2 atoms and indicated a reasonable agreement with the X-ray diffraction data. For the Co1−P and Co2−S bond distances, the same overestimation was observed as that mentioned above for mononuclear complexes. Compared to the related mononuclear complexes, the MO diagram for **3** nearly reproduces the addition of the individual MO diagrams. The HOMOs are almost identical in shape with the HOMOs of **5** and **6**. The computed spin density distribution presented in Figure 15 indicates that the unpaired spin is located on both Co(II) ions. On first inspection, powder EPR spectra and SQUID experiments indicate that both binuclear complexes **3** and **4** correspond to the superposition of the fragments developed above and EPR data were simulated with two distinct g tensors corresponding to two paramagnetic centers. Thus, for both dinuclear compounds, we started our computation on the whole molecule by replacing one Co atom with a diamagnetic Zn(II) center (d^{10}, $S = 0$) to reach individual g tensors. The g tensor extracted from EPR simulation for **3** indicates $g_x, g_y > g_z$ for Co1 and supports a low-spin ground state identical to **5**. This is in agreement with the computed g tensor obtained for the low-spin Co1 which reproduces quite satisfactory the EPR data. For the high-spin Co2, a more important discrepancy was observed between the calculated and the experimental g values.

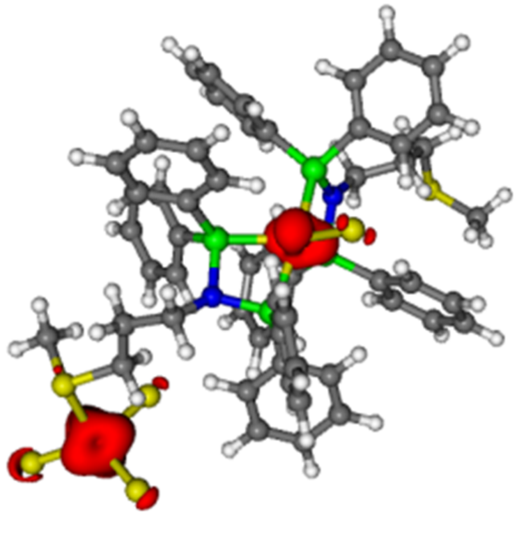

Figure 15. Spin density plots calculated for **3**.

As no X-ray structure is available for **4**, two hypotheses could be formulated (Chart 2), one compatible with a zwitterionic form similar to **3** and the other with a Co1 center associated with a $CoCl_4$ dianion. For the first hypothesis, we used the data from the crystal structure of the mononuclear Co complex **7** as a fragment to build the dinuclear complex with a similar environment for both Co atoms, as in **3** (Figure 1).

As shown in Table S2 (ESI), the calculated geometrical parameters reproduce well the experimental values obtained for **3**. The shorter distance calculated between the two metal centers compared to **4** ($\sim$1.3 Å) is consistent with the flexibility of the alkyl chains in **3**, which lead to a curved zwitterionic form. As expected, the SOMOs are localized over the cobalt ions with a small participation of the Cl, S, and P atoms as observed for **3** (Figure S23 in ESI). The computed spin density distribution for the zwitterionic form (Figure S24 in ESI) indicates that the unpaired spin is localized on both Co atoms.

Single-point analysis on the optimized structure using the method described above for **3** provides nearly axial *g* tensors very similar to those for the parent complex **7** for the low-spin Co1 and in agreement with the experimental powder EPR spectra. The results for the high-spin Co2 are more nuanced with an important discrepancy.

The second structural hypothesis, thereafter noted **4′**, was a complex where the Co1 center is associated with a $CoCl_4$ dianion. We only optimized the dication without any counterion for the low- and high-spin states configurations. The calculated geometrical parameters are given in Table S2 (ESI) for the Co1 low-spin state. In the absence of the Cl atom, the tetracoordinated Co1 could adopt a trigonal pyramidal structure because the steric bulk of the P-phenyl rings prevents a planar structure. The energy difference between the high- and the low-spin states for the anionic form is very small and in favor of the doublet by 0.5 eV. We also compared the energies of the **4′** low-spin state and **4**, which is lower by 10.6 eV. Note that the energy for the anionic form **4′** was assessed by addition of the energies of the two fragments **4′** and $CoCl_4$. Such a difference could have been expected as the gas-phase approach disfavors charged system: nothing stabilizes the cation−dianion pair. Therefore, the solid-state structure of **4** is probably best described as a zwitterionic form with a low-spin state for the Co1 atom.

■ CONCLUSION

This work has illustrated the nontrivial coordination chemistry of Co(II) complexes with two tritopic *P,P,S* ligands of the *N*-functionalized DPPA type and provided further examples of the versatile coordination geometries displayed by this metal center. As expected, the different nature of the *N*-substituent in the assembling ligands $(Ph_2P)_2N(CH_2)_3SMe$ (**1**) and $(Ph_2P)_2N(p\text{-}C_6H_4)SMe$ (**2**), an alkylthioether or an arylthioether group, respectively, has no significant impact on the *P,P*-chelating ability of these diphosphine ligands, which is their main characteristics. However, the higher flexibility of the alkylthioether *N*-substituent and its more electron-rich S atom facilitates coordination of a second metal center. Thus, the dinuclear complex **3**, which was obtained by reaction of ligand **1** with $CoCl_2$ in a 1:1 molar ratio, has an original zwitterionic structure consisting of a cationic CoCl center, bis-chelated by two PNP ligands, and one anionic $CoCl_3$ moiety linked to the *N*-thioether function. The reaction of ligand **2** with $CoCl_2$ in a 1:1 molar ratio led also to a dinuclear complex, **4**. To gain better insight into the structures and properties of these complexes, a retro-synthetic approach was developed, consisting in the synthesis of mononuclear fragments as similar as possible to those constituting the dinuclear complexes, in order to compare their spectroscopic signatures (FT-IR, UV−vis, EPR) with those of the dinuclear complex. First, this approach was successfully applied to **3**, whose spectroscopic characteristics were analyzed as the superposition of those of the corresponding mononuclear fragments. Magnetic and EPR studies and theoretical calculations were performed in order to gain a more complete understanding of the systems investigated. A combination of solution and solid-state data was used to facilitate comparisons between the molecular fragments and the dinuclear complexes and also with literature data. However, not every technique could be used both in solution and in the solid state. After validation with **3**, this "lego-type" approach was applied to complex **4**, obtained by reaction of ligand **2** with $CoCl_2$ in a 1:1 molar ratio, for which the structure could not be determined by single-crystal X-ray diffraction. We thus synthesized and characterized the complexes $[CoCl(\mathbf{2})_2]PF_6$ (**7**) and $[H\mathbf{2}']_2[CoCl_4]$ (**8**) ($\mathbf{2}' = NH_2(p\text{-}C_6H_4)SMe$) as models of the elementary bricks constitutive of **4**. Two possibilities were envisaged for the structure of **4**, a zwitterionic structure similar to that of complex **3**, or an ion pair containing a tetrahedral dicationic bis-chelated Co center associated with a $CoCl_4$ dianion. It was concluded from the spectroscopic data and DFT calculations that the former was more likely. We can anticipate that the approach developed in this work will be useful in other polynuclear systems to evaluate the degree of intramolecular cooperativity between building blocks and in complex systems for which structural information cannot always be obtained by single-crystal X-ray diffraction.

■ EXPERIMENTAL SECTION

General Procedures. All operations were carried out using standard Schlenk techniques under inert atmosphere. Solvents were purified and dried under nitrogen by conventional methods. IR spectra were recorded in the region 4000−100 cm^{-1} on a Nicolet 6700 FT-IR spectrometer (ATR mode, SMART ORBIT accessory, Diamond crystal). Elemental analyses were performed by the "Service de microanalyses", Université de Strasbourg, and by the "Service Central d'Analyse", USR-59/CNRS, Solaize. Electrospray mass spectra (ESI-MS) were recorded on a microTOF (BrukerDaltonics, Bremen, Germany) instrument using nitrogen as drying agent and nebulizing gas, and MALDI-TOF analyses were carried out on a BrukerAutiflexII TOF/TOF (BrukerDaltonics, Bremen, Germany) using dithranol (1.8.9 trihydroxyanthracene) as a matrix. All other reagents were used as received from commercial suppliers. Ligands **1** and **2** were prepared according to literature methods.

Synthesis of the Complexes. We first describe the complexes containing ligand **1** and then those with ligand **2**.

*Complex [$Co_2Cl_4(\mathbf{1})_2$] (**3**). Synthesis Resulting from the Reaction of $CoCl_2$ with Ligand **1**.* To a suspension of anhydrous $CoCl_2$ (0.082 g, 0.63 mmol) in CH_2Cl_2 (10 mL) was added a solution of ligand **1** (0.300 g, 0.63 mmol) in CH_2Cl_2 (20 mL). The solution quickly turned to green and was stirred at room temperature for 12 h. The solution was filtered through a Celite pad to ensure removal of any unreacted starting material, and the solvent was removed under reduced pressure. The resulting dark green solid was washed with diethyl ether and pentane and recrystallized from a mixture of CH_2Cl_2/pentane (1:5), yielding complex **3** (0.210 g, 55%). Yield was based on the crystalline material; however, the FTIR spectra of the green powder (precipitated or isolated after drying of the mother liquor) were similar to those of crystals of **3**. Red/green crystals suitable for single-crystal X-ray diffraction were grown from a mixture of CH_2Cl_2/pentane. Anal. Calcd for $C_{56}H_{58}Cl_4Co_2N_2P_4S_2$ (1206.78): C, 55.74; H, 4.84; N, 2.32. Found: C, 55.33; H, 4.83; N, 2.17. FTIR (ν_{max}(solid)/cm^{-1}) 1770w, 1480w, 1433s, 1310w, 1184w, 1091s, 1069sh, 1037sh, 997m, 879m, 734s, 694vs. Far-FTIR (ν_{max}(solid)/cm^{-1}) 531s, 511s, 502s, 490s, 482s, 319vs. MS (ESI): *m*/*z* (ranked by decreasing intensity) = 1005.1 $[M - H - CoCl_4]^+$, 1040.1 $[M - CoCl_3]^+$.

*Synthesis Starting from Complex **5**.* Solid anhydrous $CoCl_2$ (0.0175 g, 0.135 mmol) was added to a deep red solution of complex **5** (0.080 g, 0.067 mmol) in CH_2Cl_2 (20 mL). The resulting suspension was stirred overnight, filtered through a Celite pad to remove the "$CoCl(PF_6)$" formed, and concentrated to a quarter of its original volume under reduced pressure. Addition of pentane (50 mL) led to the precipitation of a green powder, isolated by filtration, dried under reduced pressure, and identified as complex **3** by FT-IR and EA (0.043 g, 53% based on complex **5**). FT-IR data are superimposable to those described above. Anal. Calcd: C, 55.74; H, 4.84; N, 2.32. Found: C, 55.46; H, 4.77; N, 2.29.

*Complex [CoCl(**1**)$_2$]PF$_6$ (**5**).* A solution of ligand **1** (0.500 g, 1.06 mmol) in CH_2Cl_2 (20 mL) was added to a mixture of anhydrous $CoCl_2$ (0.069 g, 0.53 mmol) and KPF_6 (0.097 g, 0.53 mmol) in CH_2Cl_2 (10 mL). The solution turned to brown and was stirred for 12 h. The solution was filtered through a Celite pad to ensure removal of any unreacted starting material, and the solvent was removed under reduced pressure. The resulting red/brown solid was washed with diethyl ether and pentane and recrystallized from a mixture of CH_2Cl_2/pentane, affording red crystals of complex **5** (0.590 g, 94%). Anal. Calcd for $C_{56}H_{58}ClCoF_6N_2P_5S_2 \cdot 3CH_2Cl_2$ (1441.25): C, 49.17; H, 4.48; N, 1.94. Found: C, 48.78; H, 4.47; N, 1.87. FTIR (ν_{max}(solid)/cm^{-1}) 1434m, 1312w, 1187w, 1091s, 999w, 834vs, 734s, 693s. Far-FTIR (ν_{max}(solid)/cm^{-1}) 556vs, 530vs, 513vs, 501vs, 490vs, 418m. MS (ESI): *m/z* 1040.2 $[M - PF_6]^+$.

*Complex [CoCl$_3$(H**1′**)] (**6**) (**1′** = NH$_2$(CH$_2$)$_3$SMe).* An aqueous HCl solution (0.40 mL of 37% HCl in H_2O, corresponding to 4.75 mmol of HCl) was added to a solution of 3-(methylthio)propylamine (0.53 mL, 0.500 g, 4.75 mmol) in CH_2Cl_2. A white precipitate was instantaneously formed. Anhydrous $CoCl_2$ (0.617 g, 4.75 mmol) was then added to the suspension, which turned blue, and the mixture was stirred for 2 h. The volatiles were then removed under reduced pressure, and the solid was washed with diethyl ether (2 × 20 mL). Complex **6** was isolated as a blue powder (1.11 g, 86%). Anal. Calcd for $C_4H_{12}Cl_3CoNS$ (271.50): C, 17.70; H, 4.45; N, 5.16. Found: C, 17.66; H, 4.75; N, 5.29. FTIR (ν_{max}(solid)/cm^{-1}) 3102s, 2941m, 1572m, 1486s, 1443m, 1244w, 1217w, 1114w, 1097m, 1040w, 978m, 932m, 827w, 773w. Far-FTIR (ν_{max}(solid)/cm^{-1}) 489w, 459w, 433w, 289vs MS (ESI): *m/z* 234.9 $[M - Cl]^+$.

*Complex [CoCl$_2$(**2**)]$_2$ (**4**).* The same procedure as for complex **3** was used with anhydrous $CoCl_2$ (0.051 g, 0.39 mmol) and ligand **2** (0.200 g, 0.39 mmol) and afforded complex **4** as green crystalline solid (0.208 g, 83%). Anal. Calcd for $C_{62}H_{54}Cl_4Co_2N_2P_4S_2$ (1274.81): C, 58.41; H, 4.27; N, 2.20. Found: C, 58.77; H, 4.54; N, 2.35. FTIR (ν_{max}(solid)/cm^{-1}) 1586w, 1491m, 1433s, 1299w, 1271w, 1217m, 1158w, 1093s, 1026w, 1010w, 998w, 934m, 894s, 811w, 736s, 691vs. Far-FTIR (ν_{max}(solid)/cm^{-1}) 554m, 526s, 495s, 423w, 295s. MS (ESI): *m/z* (ranked by decreasing intensity) = 1073.1 $[M - H - CoCl_4]^+$, 1108.1 $[M - CoCl_3]^+$.

*Synthesis Starting from Complex **7**.* The same procedure as for complex **3** was followed, with $CoCl_2$ (0.0186 g, 0.143 mmol) and complex **7** (0.090 g, 0.072 mmol) in CH_2Cl_2 (20 mL), affording complex **4** (0.057 g, 62%). FT-IR data are superimposable to those described above. Anal. Calcd: C, 58.41; H, 4.27; N, 2.20. Found: C, 58.38; H, 4.49; N, 2.30.

*Complex [CoCl(**2**)$_2$]PF$_6$ (**7**).* The same procedure as for complex **5** was used with anhydrous $CoCl_2$ (0.064 g, 0.49 mmol), KPF_6 (0.091 g, 0.49 mmol), and ligand **2** (0.500 g, 0.99 mmol) and afforded green crystals of complex **7** (0.580 g, 94%). Anal. Calcd for $C_{62}H_{54}ClCoF_6N_2P_5S_2 \cdot H_2O$ (1272.50): C, 58.52; H, 4.44; N, 2.20. Found: C, 58.60; H, 4.43; N, 1.87. FTIR (ν_{max}(solid)/cm^{-1} 1490m, 1434m, 1217m, 1094m, 937m, 898m, 836vs, 736m, 694s. Far-FTIR (ν_{max}(solid)/cm^{-1}) 556s, 526vs, 514sh, 492vs, 443m. MS (ESI): *m/z* 1108.2 $[M - PF_6]^+$.

*Complex [H**2′**]$_2$[CoCl$_4$] (**8**) (**2′** = NH$_2$(p-C$_6$H$_4$)SMe).* The same procedure as for complex **6** was used with anhydrous $CoCl_2$ (0.466 g, 3.59 mmol), aqueous HCl solution (0.29 mL of 37% HCl in H_2O, corresponding to 3.59 mmol of HCl), and 4-(methylthio)aniline (0.45 mL, 0.500 g, 3.59 mmol). Unreacted $CoCl_2$ was removed by water washing before additional Et_2O washing, and complex **8** was isolated as a blue powder (0.760 g, 44%, based on $CoCl_2$ used). Anal. Calcd for $C_{14}H_{20}Cl_4CoN_2S_2 \cdot 4H_2O$ (553.26): C, 30.39; H, 5.10; N, 5.06. Found: C, 30.26; H, 5.17; N, 4.92. FTIR (ν_{max}(solid)/cm^{-1}) 3444m, 3372m, 2989w, 2947w, 1611m, 1453s, 1402m, 1309w, 1184s, 1082w, 1034m, 1006s, 794s, 710w. Far-FTIR (ν_{max}(solid)/cm^{-1}) 322m, 294s, 272s, 226m, 168m, 125vs MS (ESI): *m/z* 140.1 $[CH_3S(C_6H_4)NH_3]^+$.

X-ray Data Collection, Structure Solution, and Refinement for All Compounds. Suitable crystals for the X-ray analysis of all compounds were obtained as described above. The intensity data were collected on a Kappa CCD diffractometer[44] (graphite monochromated Mo Kα radiation, λ = 0.71073 Å) at 173(2) K. Crystallographic and experimental details for the structures are summarized in Table S1 (ESI). The structures were solved by direct methods (SHELXS-97) and refined by full-matrix least-squares procedures (based on F^2, SHELXL-97)[45] with anisotropic thermal parameters for all the non-hydrogen atoms. The hydrogen atoms were introduced into the geometrically calculated positions (SHELXS-97 procedures) and refined *riding* on the corresponding parent atoms. For some compounds a MULTISCAN correction was applied.[46]

Magnetic Measurements. Measurements were performed on microcrystalline samples enclosed in 30 μm polyethylene bags. Weights were accurately determined with a Mettler Toledo MX5 microbalance. The bags diamagnetic contribution was subtracted from the measured magnetic moments with a diamagnetic correction combined to a small Curie tail determined previously on a massive sample. Measurements were performed on Quantum Design MPMS-5XL with a dc probe and MPMS-7 with a RSO probe SQUID magnetometers; data were corrected when necessary with locally developed procedures using multipole fitting.[47] Sample diamagnetic contributions were approximated using Pascal constants. Magnetic simulations were calculated with a locally modified version of the Magpack software.[48]

EPR measurements. X-band (Larmor frequency ≈ 9.3 GHz) EPR spectra were recorded with a continuous-wave EMXplus spectrometer (BrukerBiospin GmbH, Germany) equipped with a high-sensitivity resonator (4119HS-W1, Bruker). The spectrometer was tuned so the settings (modulation coils, incident microwave power) did not distort the EPR signal. Measurements were carried out on powdered samples held at 4−5 K. Simulations were completed with the EasySpin free software (http://www.easyspin.org).

Computational Details. Ground state electronic structures have been calculated by DFT methods using the Amsterdam Density Functional (ADF2010.02).[49] Geometry optimization was based on the hybrid B3LYP exchange-correlation functional.[50,51] A standard triple-ζ Slater basis set was used for all atoms. All calculations were performed within the unrestricted formalism. Relativistic effects were not included. The ORCA package[52] was used to calculate EPR properties through a single point on ADF-optimized geometries. B3LYP exchange-correlation functional was applied with TZVP basis[53] for the metal centers and the remaining atoms. Representations of the molecular structures and orbitals were made using ADFview v06. The obtained wave functions were analyzed with the DGRID package to compute maps of spin density.[54]

■ ASSOCIATED CONTENT

Ⓢ Supporting Information

The Supporting Information is available free of charge on the ACS Publications website at DOI: 10.1021/acs.inorgchem.5b02889.

> X-ray data collection and structure refinement for all compounds, CCDC numbers 1440248−1440252 (**3**·2(CH$_2$Cl$_2$), **4**·CH$_2$Cl$_2$, **5**, **7**, and **8**) and 1451018−1451019 (**9** and **10**·CH$_2$Cl$_2$); far-FT-IR spectra and UV−vis spectra of compounds **3**−**8**; molar susceptibility plots vs *T* and isothermal magnetization plots for compounds **3**−**8**; representation of the magnetic pair compound **5**; representation of the magnetic layers in compound **8**; relevant computed geometrical parameters for complexes **3**−**8**; ADF view drawings of the Kohn−Sham highest occupied molecular orbitals (SOMOs) of complexes **6** and **4**; spin density plots calculated for **4**; principal *g* values for complexes **5**−**8** and Zn(II) model complexes of **3** and **4** (PDF)

X-ray crystallographic data in CIF format (CIF)

AUTHOR INFORMATION

Corresponding Author

*E-mail: braunstein@unistra.fr.

Notes

The authors declare no competing financial interest.

ACKNOWLEDGMENTS

We are grateful to the CNRS, the Ministère de la Recherche (Paris), the French EPR Federation of Research (REseau NAtional de Rpe interDisciplinaire, RENARD, Fédération IR-RPE CNRS 3443), the DFH/UFA (International Research Training Group 532-GRK532, Ph.D. grant to C.F.), and the *Fundação para a Ciência e Tecnologia* (FCT) (fellowships SFRH/BPD/73253/2010 to C.F. and SFRH/BPD/44262/2008 to V.R.) for financial and scientific support. We thank Dr. L. Karmazin and Miss. C. Bailly (Service de radiocrystallographie, Institut de Chimie, Unistra) and Dr. R. Pattacini for the X-ray diffraction studies, Mélanie Boucher for technical assistance, and Dr. D. Specklin for the graphical Figures 1−5. We thank the high-performance computing center of the University of Strasbourg for computation facilities.

REFERENCES

(1) For selected reviews see, e.g., (a) Hierso, J.-C.; Amardeil, R.; Bentabet, E.; Broussier, R.; Gautheron, B.; Meunier, P.; Kalck, P. *Coord. Chem. Rev.* **2003**, *236*, 143−206. (b) Appleby, T.; Woollins, J. D. *Coord. Chem. Rev.* **2002**, *235*, 121−140. (c) Bhattacharyya, P.; Woollins, J. D. *Polyhedron* **1995**, *14*, 3367−3388. Other specific examples are cited along the manuscript.

(2) (a) Rosa, V.; Fliedel, C.; Ghisolfi, A.; Pattacini, R.; Avilés, T.; Braunstein, P. *Dalton Trans.* **2013**, *42*, 12109−12119. (b) Fliedel, C.; Pattacini, R.; Braunstein, P. *J. Cluster Sci.* **2010**, *21*, 397−415. (c) Ganesamoorthy, C.; Balakrishna, M. S.; Mague, J. T. *Inorg. Chem.* **2009**, *48*, 3768−3782. (d) Rodriguez-Zubiri, M.; Gallo, V.; Rosé, J.; Welter, R.; Braunstein, P. *Chem. Commun.* **2008**, 64−66. (e) Gallo, V.; Mastrorilli, P.; Nobile, C. F.; Braunstein, P.; Englert, U. *Dalton Trans.* **2006**, 2342−2349.

(3) (a) Lin, B.; Liu, Z.; Liu, M.; Pan, C.; Ding, J.; Wu, H.; Cheng, J. *Catal. Commun.* **2007**, *8*, 2150−2152. (b) Posset, T.; Rominger, F.; Blümel, J. *Chem. Mater.* **2005**, *17*, 586−595. (c) Schweyer-Tihay, F.; Braunstein, P.; Estournès, C.; Guille, J. L.; Lebeau, B.; Paillaud, J.-L.; Richard-Plouet, M.; Rosé, J. *Chem. Mater.* **2003**, *15*, 57−62. (d) Braunstein, P.; Kormann, H.-P.; Meyer-Zaika, W.; Pugin, R.; Schmid, G. *Chem. - Eur. J.* **2000**, *6*, 4637−4646.

(4) Fliedel, C.; Faramarzi, V.; Rosa, V.; Doudin, B.; Braunstein, P. *Chem. - Eur. J.* **2014**, *20*, 1263−1266.

(5) For recent examples see, e.g., (a) Aydemir, M.; Baysal, A.; Sahin, E.; Gümgüm, B.; Özkar, S. *Inorg. Chim. Acta* **2011**, *378*, 10−18. (b) Ganesamoorthy, C.; Balakrishna, M. S.; Mague, J. T. *J. Organomet. Chem.* **2009**, *694*, 3390−3394. (c) Ganesamoorthy, C.; Balakrishna, M. S.; Mague, J. T.; Tuononen, H. M. *Inorg. Chem.* **2008**, *47*, 7035−7047. (d) Paolillo, R.; Gallo, V.; Mastrorilli, P.; Nobile, C. F.; Rosé, J.; Braunstein, P. *Organometallics* **2008**, *27*, 741−746. (e) Gümgüm, B.; Biricik, N.; Durap, F.; Özdemir, I.; Gürbüz, N.; Ang, W. H.; Dyson, P. J. *Appl. Organomet. Chem.* **2007**, *21*, 711−715. (f) Mandal, S. K.; Gowda, G. A. N.; Krishnamurthy, S. S.; Zheng, C.; Li, S.; Hosmane, N. S. *J. Organomet. Chem.* **2003**, *676*, 22−37.

(6) For examples of Ni-based catalysts see, e.g., (a) Ghisolfi, A.; Fliedel, C.; Rosa, V.; Monakhov, K. Yu.; Braunstein, P. *Organometallics* **2014**, *33*, 2523−2534. (b) Schultz, M.; Eisenträger, F.; Regius, C.; Rominger, F.; Hanno-Igels, P.; Jakob, P.; Gruber, I.; Hofmann, P. *Organometallics* **2012**, *31*, 207−224. (c) Song, K.; Gao, H.; Liu, F.; Pan, J.; Guo, L.; Zai, S.; Wu, Q. *Eur. J. Inorg. Chem.* **2009**, *2009*, 3016−3024. (d) Lavanant, L.; Rodrigues, A.-S.; Kirillov, E.; Carpentier, J.-F.; Jordan, R. F. *Organometallics* **2008**, *27*, 2107−2117. (e) Dennett, J. N. L.; Gillon, A. L.; Heslop, K.; Hyett, D. J.; Fleming, J. S.; Lloyd-Jones, C. E.; Orpen, A. G.; Pringle, P. G.; Wass, D. F.; Scutt, J. N.; Weatherhead, R. H. *Organometallics* **2004**, *23*, 6077−6079. (f) Cooley, N. A.; Green, S. M.; Wass, D. F.; Heslop, K.; Orpen, A. G.; Pringle, P. G. *Organometallics* **2001**, *20*, 4769−4771. (g) Wass, D. F. (BP Chemicals Ltd.) WO01/10876, 2001. (h) Hofmann, P.; Perez-Moya, L. A.; Steigelmann, O.; Riede, J. *Organometallics* **1992**, *11*, 1167−1176. (i) Hofmann, P.; Perez-Moya, L. A.; Krause, M. E.; Kumberger, O.; Müller, G. Z. *Z. Naturforsch., B: J. Chem. Sci.* **1990**, *45*, 897−908.

(7) For general recent reviews on Cr-based catalysts see, e.g., (a) Dagorne, S.; Fliedel, C. *Top. Organomet. Chem.* **2013**, *41*, 125−171. (b) McGuinness, D. S. *Chem. Rev.* **2011**, *111*, 2321−2341. (c) Agapie, T. *Coord. Chem. Rev.* **2011**, *255*, 861−880. (d) van Leeuwen, P. W. N. M.; Clement, N. D.; Tschan. *Coord. Chem. Rev.* **2011**, *255*, 1499−1517. For other examples of Cr-based catalysts see, e.g., (e) Reddy Aluri, B.; Peulecke, N.; Peitz, S.; Spannenberg, A.; Müller, B. H.; Schulz, S.; Drexler, H.-J.; Heller, D.; Al-Hazmi, M. H.; Mosa, F. M.; Wöhl, A.; Müller, W.; Rosenthal, U. *Dalton Trans.* **2010**, *39*, 7911−7920. (Cr and Ni complexes): (f) Zhang, J.; Braunstein, P.; Hor, T. S. A. *Organometallics* **2008**, *27*, 4277−4279. (g) Weng, Z.; Teo, S.; Hor, T. S. A. *Dalton Trans.* **2007**, *38*, 3493−3498.

(8) Lippard, S. J.; Berg, J. M. *Principles of Bioinorganic Chemistry*; University Science Books: Mill Valley, CA, 1994; Chapter 12.

(9) (a) Raphael, A. L.; Gray, H. B. *J. Am. Chem. Soc.* **1991**, *113*, 1038−1040. (b) Geno, M. K.; Halpern, J. *J. Am. Chem. Soc.* **1987**, *109*, 1238−1240. (c) Perutz, M. F.; Fermi, G.; Luisi, B.; Shaanan, B.; Liddington, R. C. *Acc. Chem. Res.* **1987**, *20*, 309−321. (d) Halpern, J. *Science* **1985**, *227*, 869−875. (e) Garret, T. P. J.; Glingeleffer, D. J.; Guss, J. M.; Rogers, S. J.; Freeman, H. C. *J. Biol. Chem.* **1984**, *259*, 2822−2825.

(10) Ghisolfi, A.; Condello, F.; Fliedel, C.; Rosa, V.; Braunstein, P. *Organometallics* **2015**, *34*, 2255−2260.

(11) Fliedel, C.; Rosa, V.; Falceto, A.; Rosa, P.; Alvarez, S.; Braunstein, P. *Inorg. Chem.* **2015**, *54*, 6547−6559.

(12) For recent examples see, e.g., (a) Ok, F.; Aydemir, M.; Durap, F. *Appl. Organomet. Chem.* **2014**, *28*, 38−43. (b) Naik, S.; Mague, J. T.; Balakrishna, M. S. *Inorg. Chim. Acta* **2013**, *407*, 139−144. (c) Sarcher, C.; Lebedkin, S.; Kappes, M. M.; Fuhr, O.; Roesky, P. W. *J. Organomet. Chem.* **2014**, *751*, 343−350. (d) Aydemir, M.; Meric, N.; Kayan, C.; Ok, F.; Baysal, A. *Inorg. Chim. Acta* **2013**, *398*, 1−10.

(13) (a) *Catalysis without Precious Metals*; Bullock, R. M., Ed.; Wiley-VCH: Weinheim, 2010. (b) *Biochemistry and Inorganic Chemistry: Influence on Structure and Reactivity*; Swart, M., Costas, M., Eds.; John Wiley & Sons, Ltd.: Oxford, U.K., 2015. (c) Poli, R.; Allan, L. E. N.; Shaver, M. P. *Prog. Polym. Sci.* **2014**, *39*, 1827−1845. (d) Pedersen, K. S.; Bendix, J.; Clérac, R. *Chem. Commun.* **2014**, *50*, 4396−4415. (e) Grohmann, A. *Dalton Trans.* **2010**, *39*, 1432−1440. (f) Debuigne, A.; Poli, R.; Jérôme, C.; Jérôme, R.; Detrembleur, C. *Prog. Polym. Sci.* **2009**, *34*, 211−239.

(14) (a) Ghisolfi, A.; Monakhov, K.; Yu; Pattacini, R.; Braunstein, P.; López, X.; de Graaf, C.; Speldrich, M.; van Leusen, J.; Schilder, H.; Kögerler, P. *Dalton Trans.* **2014**, *43*, 7847−7859. (b) Pattacini, R.; Teo, P.; Zhang, J.; Lan, Y.; Powell, A. K.; Nehrkorn, J.; Waldmann, O.; Hor, T. S. A.; Braunstein, P. *Dalton Trans.* **2011**, *40*, 10526−10534.

(15) (a) Naktode, K.; Kottalanka, R. K.; Panda, T. K. *J. Coord. Chem.* **2014**, *67*, 3042−3053. (b) Zheng-Zhi, Z.; Ao, Yu; Hua-Ping, X.; Ru-Ji, W.; Hong-Gen, W. *J. Organomet. Chem.* **1994**, *470*, 223−229. (c) Werner, H.; Lippert, F.; Peters, K.; von Schnering, H. G. *Chem. Ber.* **1992**, *125*, 347−352.

(16) (a) Soobramoney, L.; Bala, M. D.; Friedrich, H. B. *Dalton Trans.* **2014**, *43*, 15968−15978. (b) Slepukhin, P. A.; Kim, D. M.; Charushin, V. N. *Russ. J. Coord. Chem.* **2010**, *36*, 615−617. (c) Baumann, G.; Marzilli, L. G.; Nix, C. L.; Rubin, B. *Inorg. Chim. Acta* **1983**, *77*, L35−L37.

(17) Alvarez, S.; Llunell, M. *Dalton Trans* **2000**, 3288. See also: Alvarez, S. *Chem. Rev.* **2015**, *115*, 13447−13483 and references cited therein..

(18) Ghisolfi, A.; Fliedel, C.; Rosa, V.; Pattacini, R.; Thibon, A.; Monakhov, K. Yu.; Yu; Braunstein, P. *Chem. - Asian J.* **2013**, *8*, 1795−1805.

(19) Cotton, F. A.; Wilkinson, G.; Murillo, C.; Bochmann, A. M. *Advanced Inorganic Chemistry*, 6th ed.; John Wiley & Sons: New York, 1999; pp 817−822.

(20) Li, J.; Merkel, S.; Henn, J.; Meindl, K.; Döring, A.; Roesky, H. W.; Ghadwal, R. S.; Stalke, D. *Inorg. Chem.* **2010**, *49*, 775−777.

(21) Mondal, K. C.; Samuel, P. P.; Roesky, H. W.; Carl, E.; Herbst-Irmer, R.; Stalke, D.; Schwederski, B.; Kaim, W.; Ungur, L.; Chibotaru, L. F.; Hermann, M.; Frenking, G. *J. Am. Chem. Soc.* **2014**, *136*, 1770−1773.

(22) (a) Farona, M. F.; White, J. F. *Inorg. Chem.* **1971**, *10*, 1080−1081. (b) Dyer, G.; Meek, D. W. *J. Am. Chem. Soc.* **1967**, *89*, 3983−3987.

(23) Nishida, Y.; Kida, S. *Bull. Chem. Soc. Jpn.* **1975**, *48*, 1045−1046.

(24) Pietrzyk, P.; Srebro, M.; Radoń, M.; Sojka, Z.; Michalak, A. *J. Phys. Chem. A* **2011**, *115*, 2316−2324.

(25) Marts, A. R.; Greer, S. M.; Whitehead, D. R.; Woodruff, T. M.; Breece, R. M.; Shim, S. W.; Oseback, S. N.; Papish, E. T.; Jacobsen, F. E.; Cohen, S. M.; Tierney, D. L. *Appl. Magn. Reson.* **2011**, *40*, 501−511.

(26) Bennett, B. *Curr. Top. Biophys.* **2002**, *26*, 49−57.

(27) Myers, W. K.; Duesler, E. N.; Tierney, D. L. *Inorg. Chem.* **2008**, *47*, 6701−6710.

(28) Jacobsen, F. E.; Breece, R. M.; Myers, W. K.; Tierney, D. L.; Cohen, S. M. *Inorg. Chem.* **2006**, *45*, 7306−7315.

(29) Nishida, Y.; Shimohori, H. *Bull. Chem. Soc. Jpn.* **1973**, *46*, 2406−2410.

(30) Figgis, B. N.; Hitchman, M. A. *Ligand Field Theory and Its Applications*; Wiley-VCH.: New York, 2000; pp 228−263.

(31) Banci, L.; Bencini, A.; Benelli, C.; Gatteschi, D.; Zanchini, C. *Struct. Bonding (Berlin)* **1982**, *52*, 37−86.

(32) Cossee, P.; van Arkel, A. E. *J. Phys. Chem. Solids* **1960**, *15*, 1−6.

(33) DeW, W.; Horrocks, D. A., Jr.; Burlone. *J. Am. Chem. Soc.* **1976**, *98*, 6512−6516.

(34) Dyrek, K.; Dyrek, M.; Wesełucha-Birczyńska, A. *Polyhedron* **1985**, *4*, 169−172.

(35) Qu, T.; Kuang, X.-Y.; Li, Y.-F.; Chai, R.-P. *Chem. Phys. Lett.* **2011**, *504*, 170−174.

(36) Boča, R. *Theoretical foundations of Molecular Magnetism*; Elsevier: Lausanne (Switzerland), 1999; Chapters 5 and 9.

(37) Hamiltonian$\hat{H} = \beta g \sum \hat{S}\cdot\hat{H} - 2J\hat{S}_1\hat{S}_2 + \sum D\hat{S}_z^2 + E(\hat{S}_x^2 - \hat{S}_y^2)$

(38) $\theta = \frac{z2JS(S+1)}{3k}$

(39) It must be noted that an uncorrected ferromagnetic impurity would give a similar contribution than a very high TIP, but magnetization measurements at 100 K did not evidence such an impurity.

(40) Though no maximum is observed on the susceptibility plot, a similar behavior was observed for the isothermal magnetization of a 2D Heisenberg honeycomb lattice model, see: Curély, J.; Lloret, F.; Julve, M. *Phys. Rev. B: Condens. Matter Mater. Phys.* **1998**, *58*, 11465−11483.

(41) Only visual agreement was sought for. Since parameters are likely to be heavily correlated, the parameters are certainly neither unique nor optimal.

(42) (a) Drago, R. S.; Stahlbush, J. R.; Kitko, D. J.; Breese, J. *J. Am. Chem. Soc.* **1980**, *102*, 1884−1889. (b) Stelzer, O.; Sheldrick, W. S.; Subramanian, J. *J. Chem. Soc., Dalton Trans.* **1977**, 966−970.

(43) (a) Krzystek, J.; Ozarowski, A.; Zvyagin, S. A.; Telser, J. *Inorg. Chem.* **2012**, *51*, 4954−4964. (b) Krzystek, J.; Zvyagin, S. A.; Ozarowski, A.; Fiedler, A. T.; Brunold, T. C.; Telser, J. *J. Am. Chem. Soc.* **2004**, *126*, 2148−2155. (c) Romerosa, A.; Saraiba-Bello, C.; Serrano-Ruiz, M.; Caneschi, A.; Mckee, V.; Peruzzini, M.; Zanobini, F. *Dalton Trans.* **2003**, 3233−3239. (d) Makinen, M. W.; Kuo, L. C.; Yim, M. B.; Wells, G. B.; Fukuyama, J. M.; Kim, J. E. *J. Am. Chem. Soc.* **1985**, *107*, 5245−5255.

(44) Bruker-Nonius. *Kappa CCD Reference Manual*; Nonius BV: The Netherlands, 1998.

(45) Sheldrick, G. M. *Acta Crystallogr., Sect. A: Found. Crystallogr.* **2008**, *64*, 112−122.

(46) (a) Spek, L. *J. Appl. Crystallogr.* **2003**, *36*, 7−13. (b) Blessing, B. *Acta Crystallogr., Sect. A: Found. Crystallogr.* **1995**, *51*, 33−38.

(47) Palamarciuc, T.; Oberg, J. C.; El Hallak, F.; Hirjibehedin, C. F.; Serri, M.; Heutz, S.; Létard, J.-F.; Rosa, P. *J. Mater. Chem.* **2012**, *22*, 9690−9695.

(48) Borrás-Almenar, J. J.; Clemente-Juan, J. M.; Coronado, E.; Tsukerblat, B. S. *Inorg. Chem.* **1999**, *38*, 6081−6088; and *J. Comput. Chem.* **2001**, *22*, 985−991.

(49) *ADF2010.02*; Theoretical Chemistry, Vrije Universiteit: Amsterdam, The Netherlands, SCM, 2010.

(50) Becke, A. D. *J. Chem. Phys.* **1993**, *98*, 5648−5652.

(51) Lee, C.; Yang, W.; Parr, R. G. *Phys. Rev. B: Condens. Matter Mater. Phys.* **1988**, *37*, 785−789.

(52) (a) Neese, F. *ORCA An Ab Initio, DFT and Semiempirical Electronic Structure Package*, version 2.9.1; Universität Bonn: Bonn, Germany, 2012. (b) Neese, F. *J. Chem. Phys.* **2007**, *127*, 164112.

(53) (a) Schäfer, A.; Horn, H.; Ahlrichs, R. *J. Chem. Phys.* **1992**, *97*, 2571−2577. (b) Schäfer, A.; Huber, C.; Ahlrichs, R. *J. Chem. Phys.* **1994**, *100*, 5829−5835.

(54) Kohout, M.*DGrid*, version 4.6; Radebeul, 2011.

DOI: 10.1021/acs.inorgchem.5b02889
Inorg. Chem. XXXX, XXX, XXX−XXX